
Conditioning Sparse Variational Gaussian Processes for Online Decision-making

Wesley J. Maddox
New York University
wj363@nyu.edu

Samuel Stanton
New York University
ss13641@nyu.edu

Andrew Gordon Wilson
New York University
andrewgw@cims.nyu.edu

Abstract

With a principled representation of uncertainty and closed form posterior updates, Gaussian processes (GPs) are a natural choice for online decision making. However, Gaussian processes typically require at least $\mathcal{O}(n^2)$ computations for n training points, limiting their general applicability. Stochastic variational Gaussian processes (SVGPs) can provide scalable inference for a dataset of fixed size, but are difficult to efficiently condition on new data. We propose online variational conditioning (OVC), a procedure for efficiently conditioning SVGPs in an online setting that does not require re-training through the evidence lower bound with the addition of new data. OVC enables the pairing of SVGPs with advanced look-ahead acquisition functions for black-box optimization, even with non-Gaussian likelihoods. We show OVC provides compelling performance in a range of applications including active learning of malaria incidence, and reinforcement learning on MuJoCo simulated robotic control tasks.

1 Introduction

Intelligent systems should be able to quickly and efficiently adapt to new data, adjusting their prior beliefs in response to the most recent events. These characteristics are desirable whether the system in question is controlling the actuators of a robot, tuning the power output of a laser, or monitoring the changing preferences of users on an online platform. What these applications share in common is a constant stream of new information. In this paper, we are interested in efficient *conditioning*, meaning that we wish to efficiently update a posterior distribution after receiving new data.

The ability of Gaussian process (GP) regression models to condition on new data in closed form has made them a popular choice for Bayesian optimization (BO), active learning, and control [24]. All of these settings share similar characteristics: there is an “outer loop”, where new data is acquired from the real world (e.g. an expensive simulator), interleaved with an “inner loop”, which chooses where to collect data. In BO, for example, the “inner loop” is the optimization of an acquisition function evaluated using a surrogate model of the true objective. Simple acquisition functions, e.g. expected improvement (EI), consider only the current state of the surrogate, while more sophisticated acquisition functions “look ahead” to consider the effect of hypothetical observations on future surrogate states. One such acquisition function, batch knowledge gradient (qKG), defines the one-step Bayes-optimal data batch as the batch that maximizes the expected surrogate maximum *after* the batch has been acquired [2, 84]. Advanced acquisition functions like qKG require the surrogate to have both efficient posterior sampling and efficient conditioning on new data.

GP regression has two major limitations that have prevented its large scale deployment for online decision-making. First, the computational and memory consumption of exact GPs grows at least quadratically with the amount of data [25, 65], generally limiting their usage to BO problems with fewer than 1,000 function evaluations [24, 2, 79]. Second, they are limited to applications that have continuous real-valued responses, enabling modelling with solely a Gaussian likelihood. Stochastic

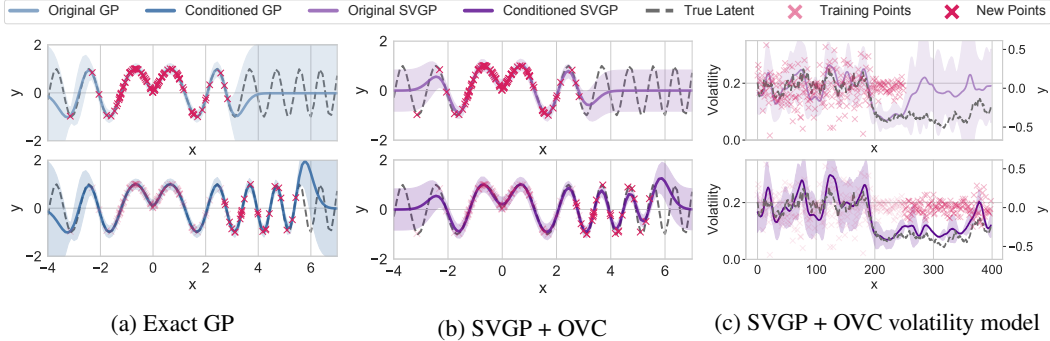


Figure 1: An exact GP updates its predictive distribution after conditioning on new data points (a, moving from top row to bottom row). With OVC, we can condition SVGPs on both Gaussian responses (b) and non-Gaussian models (c) such as the Gaussian copula volatility model [82].

variational Gaussian processes (SVGPs) [33] have constant computational and memory footprints and are applicable to non-Gaussian likelihoods, but they sacrifice closed form expressions for updated posteriors on receiving new data. The SVGP posterior is *optimized* through the evidence lower bound (ELBO). In the online setting, training with the ELBO has two primary difficulties: the need to specify a fixed number of observations to properly scale the ELBO gradient [8] and the need to adjust the inducing points without looking at past data [3, 9]. Thus, we are presented with a choice between the simplicity and analytic tractability of exact GPs and the scalability and flexibility of SVGPs.

In this work, we develop **Online Variational Conditioning (OVC)** to allow SVGPs to be conditioned on-the-fly, as shown in Figure 1. In the top row of each subplot, we fit the data points shown in red, shifting to another batch of data points in the bottom row. We use an exact GP in Figure 1a, with exact conditioning shown in the bottom panel. The SVGP emulates the exact GP very well before seeing the new data and again after conditioning on the new data by using OVC (Figure 1b). In Figure 1c, we consider a non-Gaussian data model (a Gaussian copula volatility model [82]), where we cannot use exact GPs; the SVGP is still able to update its posterior over the latent volatility in response to new data without “forgetting” old observations. OVC is inspired by a new, simple rederivation of streaming sparse GPs (O-SGPR), originally proposed by Bui et al. [9]. OVC makes SVGPs truly compelling models for online decision-making, augmenting their existing strengths with efficient, closed-form conditioning on new data points. In short, our contributions are:

- The development of OVC, a novel method to condition SVGPs on new data without re-optimizing the variational posterior through an evidence lower bound.
- OVC provides both stable inducing point initialization for SVGPs while enabling the inducing points and variational parameters to update in response to the new data.
- Enabling the effective application of SVGPs, through OVC, in look-ahead acquisitions in BO for black-box optimization, controlling dynamical systems, and active learning.

Please see Appendix A for discussion of the limitations and broader impacts of our work. Our code is available at https://github.com/wjmaddox/online_vargp.

2 Preliminaries and Related Work

In this section, we first review exact inference with Gaussian processes before reviewing variational sparse Gaussian processes, introducing sparse Gaussian process regression (SGPR), sparse variational Gaussian processes (SVGP), and streaming sparse GPs (O-SGPR). Please see Appendix B for further background and Appendix B.1 specifically for further related work.

2.1 Gaussian Processes and Exact Inference

For a full introduction to GPs, see Rasmussen and Williams [65]. We begin by reviewing GP regression, with inputs $\mathbf{x} \in \mathcal{X}$ and responses $y \in \mathbb{R}$. GP regression assumes $y \sim \mathcal{N}(f, \sigma^2)$, where

$f \sim \mathcal{GP}(0, k_\theta(\mathbf{x}, \mathbf{x}'))$ is a GP characterized by the kernel function k_θ and corresponding hyperparameters θ . Given $X_{\text{train}} = [\mathbf{x}_1, \dots, \mathbf{x}_n]^\top$ and $X_{\text{test}} = [\mathbf{x}'_1, \dots, \mathbf{x}'_k]^\top$, we denote the corresponding function values as $\mathbf{v} = [f(\mathbf{x}_1), \dots, f(\mathbf{x}_n)]^\top$ and $\mathbf{w} = [f(\mathbf{x}'_1), \dots, f(\mathbf{x}'_k)]^\top$, respectively. Note that \mathbf{v} and \mathbf{w} are random variables with prior covariance $\text{Cov}[\mathbf{v}, \mathbf{w}] = K_{\mathbf{vw}} := k_\theta(X_{\text{train}}, X_{\text{test}})$. A well-known identity for multivariate conditional Gaussians allows us to compute the GP predictive posterior $p(\mathbf{w}|X_{\text{test}}, \mathcal{D}, \theta) = \mathcal{N}(\mu_{\mathbf{w}|\mathcal{D}}^*, \Sigma_{\mathbf{w}|\mathcal{D}}^*)$ as follows:

$$\mu_{\mathbf{w}|\mathcal{D}}^* = K_{\mathbf{vw}}(K_{\mathbf{vv}} + \sigma^2 I)^{-1} \mathbf{y}, \quad \Sigma_{\mathbf{w}|\mathcal{D}}^* = K_{\mathbf{ww}} - K_{\mathbf{vw}}(K_{\mathbf{vv}} + \Sigma_{\mathbf{y}})^{-1} K_{\mathbf{vw}}, \quad (1)$$

where $\mathcal{D} := (X_{\text{train}}, \mathbf{y})$ and $\Sigma_{\mathbf{y}} = \sigma^2 I$.

Naïvely, computations with $K_{\mathbf{vv}}$ cost $\mathcal{O}(n^2)$ space and $\mathcal{O}(n^3)$ operations. When repeatedly computing $p(\mathbf{w}|X_{\text{test}}, \mathcal{D}, \theta)$ at different sets of query points X_{test} , it is more efficient to cache the terms which depend only on the training data.¹ Specifically, we store $\mathbf{a} := (K_{\mathbf{vv}} + \Sigma_{\mathbf{y}})^{-1} \mathbf{y}$ (the predictive mean cache) and $RR^\top := (K_{\mathbf{vv}} + \Sigma_{\mathbf{y}})^{-1}$ (the predictive covariance cache), resulting in simplified forms for the predictive distribution, $\mu_{\mathbf{w}|\mathcal{D}}^* = K_{\mathbf{vw}} \mathbf{a}$ and $\Sigma_{\mathbf{w}|\mathcal{D}}^* = K_{\mathbf{ww}} - K_{\mathbf{vw}} RR^\top K_{\mathbf{vw}}$. Adding a new observation is equivalent to adding a single row and column to $K_{\mathbf{vv}}$ and an entry to \mathbf{y} , which enables efficient low-rank updates to the predictive caches [58, 25, 64, 39].²

2.2 Variationally Sparse Gaussian Processes

Variational sparse GPs reduce the computational burden of GP inference through sparse approximations of the kernel matrix. For further reference, see Matthews [50] and Van der Wilk [77]. These methods define a variational distribution ϕ over the inducing point values $\mathbf{u} = [f(\mathbf{z}_1), \dots, f(\mathbf{z}_p)]^\top$, defined at inducing point locations $Z = [\mathbf{z}_1, \dots, \mathbf{z}_p]^\top$, where $\mathbf{z}_i \in \mathcal{X}$. $\phi(\mathbf{u})$ is parameterized as a Gaussian with variational mean and covariance $\mathbf{m}_{\mathbf{u}}$ and $S_{\mathbf{u}}$. These methods assume the latent function values $f(\mathbf{x}), f(\mathbf{x}')$ are conditionally independent given \mathbf{u} and $\mathbf{x}, \mathbf{x}' \notin Z$, so as to cheaply approximate the predictive posterior $p(\mathbf{w}|X_{\text{test}}, \mathcal{D}, \theta) \approx q(\mathbf{w}) = \mathcal{N}(\mu_{\mathbf{w}|\phi}^*, \Sigma_{\mathbf{w}|\phi}^*)$. Like exact GP regression, we can compute $q(\mathbf{w})$ in closed form (given $\mathbf{m}_{\mathbf{u}}, S_{\mathbf{u}}$),

$$\mu_{\mathbf{w}|\phi}^* := K_{\mathbf{wu}} K_{\mathbf{uu}}^{-1} \mathbf{m}_{\mathbf{u}}, \quad \Sigma_{\mathbf{w}|\phi}^* := K_{\mathbf{ww}} - K_{\mathbf{wu}} K_{\mathbf{uu}}^{-1} (K_{\mathbf{uu}} - S_{\mathbf{u}}) K_{\mathbf{uu}}^{-1} K_{\mathbf{uw}}. \quad (2)$$

Similarly the predictive mean and covariance caches are given by $\mathbf{a} = K_{\mathbf{uu}}^{-1} \mathbf{m}_{\mathbf{u}}$ and $RR^\top = K_{\mathbf{uu}}^{-1} (K_{\mathbf{uu}} - S_{\mathbf{u}}) K_{\mathbf{uu}}^{-1}$, reducing the complexity of inference from $\mathcal{O}(n^3)$ to $\mathcal{O}(np^2)$, which is a significant improvement if $p \ll n$.

There are two common approaches to finding optimal variational parameters $\mathbf{m}_{\mathbf{u}}$ and $S_{\mathbf{u}}$. In seminal work, Titsias [73] proposed sparse GP regression (SGPR), which optimizes $\mathbf{m}_{\mathbf{u}}$ and $S_{\mathbf{u}}$ in closed form, resulting in a "collapsed" evidence lower bound³ (ELBO) that only depends on θ and Z . The computational cost of each gradient update to the remaining model parameters is still linear in n , and like exact GP regression, SGPR requires a Gaussian likelihood. Stochastic variational GPs (SVGPs) remedies both these limitations by using gradient-based optimization to learn $\mathbf{m}_{\mathbf{u}}$ and $S_{\mathbf{u}}$ alongside Z and θ [33, 34]. The SVGP objective is an "uncollapsed" ELBO which decomposes additively across the training examples, allowing gradients to be estimated from minibatches of data, reducing the complexity of each gradient update to $\mathcal{O}(bp^2 + p^3)$, where b is the minibatch size.

We emphasize the distinction between constant-time minibatch gradients, and constant-time conditioning. Given an SVGP already trained on some existing data, conditioning jointly on both the old and new data requires storing all the data and making multiple gradient updates to the variational parameters. As the size of the dataset grows, so does the number of gradient steps needed. In contrast by constant-time conditioning we mean a procedure that takes a posterior conditioned on existing data and produces a new posterior conditioned jointly on the old and new data with a fixed amount of compute and memory, regardless of the number of past observations.

One example of constant-time conditioning is found in Bui et al. [9], who proposed streaming sparse GPs (which we call online SGPR, or O-SGPR, to distinguish from sparse spectrum GPs [44]) for

¹ Cached expressions will be written in orange

² What we use as the SGPR covariance cache is slightly different from the implementation in the prediction strategy in GPyTorch, which stores $R = K_{\mathbf{vu}} K_{\mathbf{uu}}^{-1/2}$. However, they reduce to the same strategy.

³ A lower bound of the true GP marginal log-likelihood

Algorithm 1 Online Variational Conditioning (OVC)

- Input:** Data batch $(X_{\text{batch}}, \mathbf{y})$, SVGP with inducing points Z' and $\phi(\mathbf{u}') = \mathcal{N}(\mathbf{m}_{\mathbf{u}'}, S_{\mathbf{u}'})$.
1. Compute \mathbf{c}', C' (Eq. 5).
 2. Compute $\hat{\mathbf{y}} = K'_{\mathbf{u}'\mathbf{u}'} C'^{-1} \mathbf{c}'$ and $\Sigma_{\hat{\mathbf{y}}} = K'^{-1}_{\mathbf{u}'\mathbf{u}'} C' K'^{-1}_{\mathbf{u}'\mathbf{u}'}$ (Eq. 8).
 3. Construct GP with $\mathcal{D} = ([X_{\text{batch}} \ Z'], [\mathbf{y} \ \hat{\mathbf{y}}])$ and $\Sigma = \text{blkdiag}(\Sigma_{\mathbf{y}}, \Sigma_{\hat{\mathbf{y}}})$.
 4. Compute predictive mean and covariance caches, \mathbf{a} and RR^T as in Section 2.1.
 5. Use caches to compute conditioned GP posterior on test points, X_{test} .
-

incremental learning. We extend their work, providing an alternative, simpler derivation of their model that highlights the connection with SGPR [73]. Furthermore, our perspective enables us to construct a principled approach to updating inducing point locations as new data arrives, that prevents the “forgetting” of old data induced by the resampling heuristic used by Bui et al. [9].

2.3 Bayesian Optimization and Monte Carlo Acquisitions

Bayesian optimization (BO) obtains $\mathbf{x}^* = \text{argmin}_{\mathbf{x} \in \mathcal{X}} f(\mathbf{x})$ by constructing a probabilistic *surrogate model* of f , which in turn is used to evaluate an acquisition function. GPs are favored for BO due to their sample-efficiency and efficient posterior sampling that enables cheap, gradient based optimization of the acquisition function to propose new query points [24]. Many interesting acquisition functions look ahead into the future to see how the model will change if we query a specific point, a procedure known as “fantasization” [32, 84, 39]. Fantasization is done by drawing samples from the current surrogate posterior at some set of points and conditioning the surrogate on those samples. For example, the batch knowledge gradient [qKG, 84, 2] is given by

$$a(\mathbf{x}, \mathcal{D}) := \mathbb{E}_{f(\mathbf{x}) \sim p(\cdot|\mathcal{D})} \left(\max_{\mathbf{x}' \in \mathcal{X}} \mathbb{E}_{f(\mathbf{x}') \sim p(\cdot|\mathcal{D}_{+\mathbf{x}})} f(\mathbf{x}') \right) - \max_{\mathbf{x}' \in \mathcal{X}} \mathbb{E}_{f(\mathbf{x}') \sim p(\cdot|\mathcal{D})} f(\mathbf{x}'), \quad (3)$$

where $\mathcal{D}_{+\mathbf{x}} := \mathcal{D} \cup \{(\mathbf{x}, f(\mathbf{x}))\}$. The inner expectation in the first term requires conditioning the surrogate model on posterior samples at \mathbf{x} , before optimizing through predictions of the conditioned surrogate model. The goal is to simulate the effect on the model if we had observed the batch of data.

Use of sparse GPs in BO: Sparse GPs have not seen wide adoption in the BO community, with only several preliminary studies that have mostly used basic acquisitions. Nickson et al. [55] and Krityakierne and Ginsbourger [43] used expected improvement (EI) with SGPR on several test problems, while McIntire et al. [51] proposed a sparse GP method using EI to tune free electron lasers [20]. Stanton et al. [70] proposed WISKI, an online implementation of a scalable kernel approach called SKI [83], for low-dimensional BO problems using batch upper confidence bound (qUCB) [2].

3 Methodology

We now briefly describe the key ideas behind OVC with the goal of devising an efficient and stable method for updating the variational parameters with respect to newly observed data. We begin by highlighting an alternative parameterization of SGPR that will prove useful. Then we describe the OVC update to the variational distribution from two equivalent points of view, namely the *projection view* and the *pseudo-data view*. The pseudo-data view is summarized in Algorithm 1. Next we address a critical detail for good performance, which is how the inducing point locations should be selected. We then demonstrate how OVC can be applied to compute updated posterior distributions, e.g. $p(f|\mathcal{D}_{+\mathbf{x}})$ in Eq. 3, and quantities of the posterior, during gradient-based acquisition function optimization in BO, with reference to how this can be performed practically in Section 4. Finally, we discuss how to apply OVC to models with non-Gaussian likelihoods.

3.1 Updating the Variational Posterior

We assume that we have trained a SVGP model (e.g. with the ELBO) on a fixed set of data and have already trained the inducing point locations and variational parameters, $\mathbf{m}_{\mathbf{u}}, S_{\mathbf{u}}$. Instead of the traditional $\mathbf{m}_{\mathbf{u}}, S_{\mathbf{u}}$ parameterization used by Titsias [73], Hensman et al. [33, 34], we focus for now on an alternative parameterization which was favored in early work on sparse GP inference

[67, 57]. The parameterization is also similar to those used in both dual space functional variational inference [41] and expectation propagation [10]. More recently, Panos et al. [61] used a similar parameterization in the context of large scale multi-label learning with SVGPs.

The SGPR predictive posterior $q(\mathbf{w})$ relies on two terms dependent on the training data,

$$\mathbf{c} = K_{\mathbf{u}\mathbf{v}}\Sigma_{\mathbf{y}}^{-1}\mathbf{y}, \quad C = K_{\mathbf{u}\mathbf{v}}\Sigma_{\mathbf{y}}^{-1}K_{\mathbf{v}\mathbf{u}}, \quad (4)$$

where $\Sigma_{\mathbf{y}}$ is the covariance of the likelihood $p(\mathbf{y}|\mathbf{f})$. The optimal $\mathbf{m}_{\mathbf{u}}$, $S_{\mathbf{u}}$ are then given by

$$\mathbf{m}_{\mathbf{u}} = K_{\mathbf{u}\mathbf{u}}(K_{\mathbf{u}\mathbf{u}} + C)^{-1}\mathbf{c}, \quad S_{\mathbf{u}} = K_{\mathbf{u}\mathbf{u}}(K_{\mathbf{u}\mathbf{u}} + C)^{-1}K_{\mathbf{u}\mathbf{u}}, \quad (5)$$

which can be substituted into Eq. (2) to obtain $q(\mathbf{w})$. Our first observation is that if $\Sigma_{\mathbf{y}}$ is block-diagonal, then \mathbf{c} and C are additive across blocks of observations. For some intuition, consider i.i.d. Gaussian noise (i.e. $\Sigma_{\mathbf{y}} = \sigma^2 I_n$), which implies

$$\begin{aligned} \mathbf{c}_i &= \sum_j \sigma^{-2} y_j k_{\theta}(\mathbf{z}_i, \mathbf{x}_j) = \phi(\mathbf{z}_i)^{\top} \sum_j \sigma^{-2} y_j \phi(\mathbf{x}_j), \\ C_{ik} &= \sum_j \sigma^{-2} k_{\theta}(\mathbf{z}_i, \mathbf{x}_j) k(\mathbf{x}_j, \mathbf{z}_k) = \phi(\mathbf{z}_i)^{\top} \sum_j \sigma^{-2} \phi(\mathbf{x}_j) \phi(\mathbf{x}_j)^{\top} \phi(\mathbf{z}_k), \end{aligned}$$

where ϕ is the (potentially infinite-dimensional) feature map associated with k_{θ} . Hence the entries of \mathbf{c} and C are both inner products between projected inducing points and weighted sums of features. For fixed inducing points, Z , and hyper-parameters θ , we can use these updates to produce a streaming version of SGPR by exploiting the additive structure of \mathbf{c} and C . Furthermore, this streaming version of SGPR is exactly Gaussian conditioning for SGPR as we show in Appendix C.1. We can also allow the inducing points and hyper-parameters to vary, which we address next.⁴

The projection view: We assume we have $\mathbf{c}' = K'_{\mathbf{u}'\mathbf{v}'}\Sigma_{\mathbf{y}'}^{-1}\mathbf{y}'$ and $C' = K'_{\mathbf{u}'\mathbf{v}'}\Sigma_{\mathbf{y}'}^{-1}K'_{\mathbf{v}'\mathbf{u}'}$, computed with inducing point locations Z' from data $(X'_{\text{batch}}, \mathbf{y}')$ with kernel hyperparameters θ' (using shorthand $k_{\theta'} = K'$).⁵ After obtaining the next parameters Z and θ (perhaps from gradient based optimization of the ELBO), we observe new data $(X_{\text{batch}}, \mathbf{y})$ and would like to continue with inference. One challenge is translating \mathbf{c}' , C' (whose elements are inner products of the old features) to the new feature space associated with θ . To resolve this challenge, we construct a representative set of responses, $\hat{\mathbf{y}} = P^{\top}\mathbf{c}'$ and likelihood covariance $\hat{\Sigma}_{\hat{\mathbf{y}}} = P^{\top}C'P$ to project from the old feature space into the new feature space by passing back through data space. The choice that minimizes reconstruction error is the pseudo-inverse $P = (K'_{\mathbf{v}'\mathbf{u}'}K'_{\mathbf{u}'\mathbf{v}'})^{-1}K'_{\mathbf{v}'\mathbf{u}'}$, but requires storage of the full dataset, $(X'_{\text{batch}}, \mathbf{y}')$. Instead we take $P = K'^{-1}_{\mathbf{u}'\mathbf{u}'}$, resulting in the following modifications to Eq. (4):

$$\mathbf{c} = K_{\mathbf{u}\mathbf{v}}\Sigma_{\mathbf{y}}^{-1}\mathbf{y} + K_{\mathbf{u}\mathbf{u}'}K'^{-1}_{\mathbf{u}'\mathbf{u}'}\mathbf{c}', \quad (6)$$

$$C = K_{\mathbf{u}\mathbf{v}}\Sigma_{\mathbf{y}}^{-1}K_{\mathbf{v}\mathbf{u}} + K_{\mathbf{u}\mathbf{u}'}(K'^{-1}_{\mathbf{u}'\mathbf{u}'}C'K'^{-1}_{\mathbf{u}'\mathbf{u}'})K_{\mathbf{u}\mathbf{u}'}, \quad (7)$$

Note that $K'^{-1}_{\mathbf{u}'\mathbf{u}'}\mathbf{c}' = \Sigma_{\mathbf{y}'}^{-1}\mathbf{y}'$ and $K'^{-1}_{\mathbf{u}'\mathbf{u}'}C'K'^{-1}_{\mathbf{u}'\mathbf{u}'} = \Sigma_{\mathbf{y}'}^{-1}$ in the special case where $X'_{\text{batch}} = Z'$. We also want to emphasize that although we have only considered two batches of data for the sake of clarity, the approach applies to any number of incoming batches.

The pseudo-data view: The above update is equivalent to having an SGPR model with a Gaussian likelihood with covariance $\Sigma = \text{blkdiag}(\Sigma_{\hat{\mathbf{y}}}, \Sigma_{\mathbf{y}})$ on the data $\{\text{cat}(Z', X_{\text{batch}}), \text{cat}(\hat{\mathbf{y}}, \mathbf{y})\}$, where

$$\hat{\mathbf{y}} = K'_{\mathbf{u}'\mathbf{u}'}C'^{-1}\mathbf{c}', \quad \Sigma_{\hat{\mathbf{y}}}^{-1} = K'^{-1}_{\mathbf{u}'\mathbf{u}'}C'K'^{-1}_{\mathbf{u}'\mathbf{u}'}. \quad (8)$$

This interpretation is reminiscent of prior online variational approaches of Csató and Opper [16] and Opper [56]. That is, in the context of conditioning a SVGP, we can assume that we began with data $\{Z', \hat{\mathbf{y}}\}$ and are now observing the new data $\{X_{\text{batch}}, \mathbf{y}\}$. See Appendix C.2 for a more details.

Extending to SVGPs: SGPR computes $\mathbf{m}_{\mathbf{u}}$ and $S_{\mathbf{u}}$ as a function of \mathbf{c} and C in Eq. (5). However the equations can be reversed to solve for \mathbf{c} and C given $\mathbf{m}_{\mathbf{u}}$ and $S_{\mathbf{u}}$, allowing us to condition *any* variational sparse GP into an SGPR model, without touching any previous observations due to the

⁴For full generality, we allow the hyper-parameters to vary; however, in our BO experiments, we only consider varying the inducing points as that's all we need to update when computing acquisition functions.

⁵Cached computations that depend on $(X'_{\text{batch}}, \mathbf{y}')$ are highlighted in blue.

conditional independence assumptions of variationally sparse GPs.⁶ Note that if the variational parameters are not at the optimal solution when the variational distribution is projected back to the pseudo-data, the projection will be to the targets and likelihood *for which the current variational parameters would be optimal*, which may not correspond well to the data that originally created the model. This potential pitfall is mitigated if the variational parameters are well optimized and is offset by the practical advantages of SVGPs.

Connection to O-SGPR [9]: Formally, the updates described in Eqs. (6) and (7) are equivalent to the O-SGPR approach of Bui et al. [9], as we show in Appendix C.2. The original derivation of O-SGPR is very technical, and does not highlight the similarities between the batch and online SGPR variants. Both the projection and pseudo-data views we have just described provide a much more intuitive way to reason about the behavior of O-SGPR models. Our formulation also eliminates a matrix subtraction operation, which is beneficial for numerical stability.

3.2 Inducing Point Selection

Here, we describe inducing point selection during the conditioning procedure to enable better variance reduction on new inputs. While heuristics including re-sampling [9] and data sufficient statistics [35] have been proposed, they either require the number of inducing points to grow or gradually forget old observations. We show in Appendix C.4 that relying exclusively on gradient-based optimization of inducing locations works very poorly in the online setting.

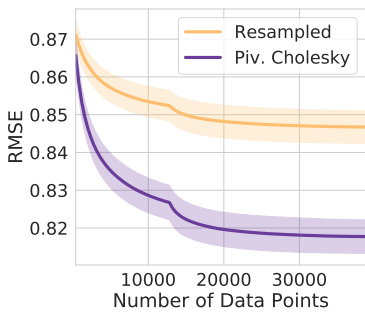


Figure 2: Incremental learning RMSE on the UCI *protein* dataset. Pivoted cholesky initialization outperforms resampling.

To update the inducing point locations during conditioning, we extend Burt et al. [11]’s batch inducing point initialization approach to heteroskedastic Gaussian likelihoods. They consider theoretical bounds on the marginal likelihood, finding that for homoscedastic Gaussian likelihoods a good strategy is to minimize the trace of the error of a rank- p Nyström approximation, e.g. $\varepsilon = \text{tr} \left(\Sigma_{\mathbf{y}}^{-1/2} (K_{\mathbf{v}\mathbf{v}} - K_{\mathbf{v}\mathbf{u}} K_{\mathbf{u}\mathbf{u}}^{-1} K_{\mathbf{u}\mathbf{v}}) \Sigma_{\mathbf{y}}^{-1/2} \right) = \sigma^{-1/2} \text{tr} (K_{\mathbf{v}\mathbf{v}} - Q_{\mathbf{v}\mathbf{v}})$ for $Q_{\mathbf{v}\mathbf{v}} = K_{\mathbf{v}\mathbf{u}} K_{\mathbf{u}\mathbf{u}}^{-1} K_{\mathbf{u}\mathbf{v}}$. They follow a classical approach of Fine and Scheinberg [23] by a greedy minimization strategy: choosing as inducing points the pivots of a rank p pivoted Cholesky factorization of $K_{\mathbf{v}\mathbf{v}}$.

We denote the function values over the batch+pseudo dataset as $\hat{\mathbf{v}} = [f(\mathbf{x}_1), \dots, f(\mathbf{x}_b), f(\mathbf{z}'_1), \dots, f(\mathbf{z}'_p)]^\top$. In our case the covariance of the pseudo-likelihood is no longer homoscedastic, so the slack term becomes $\varepsilon = \text{tr}(\Sigma^{-1/2}(K_{\hat{\mathbf{v}}\hat{\mathbf{v}}} - Q_{\hat{\mathbf{v}}\hat{\mathbf{v}}})\Sigma^{-1/2})$ and hence the pivoted Cholesky decomposition is instead performed over $\Sigma^{-1/2} K_{\hat{\mathbf{v}}\hat{\mathbf{v}}} \Sigma^{-1/2}$ to select the top p pivots of the $p + n_{\text{new}}$ matrix. When compared to re-sampling the inducing points [9], pivoted cholesky updates perform significantly better, as shown in Figure 2 on the UCI protein dataset [19]. Experimental details are given in Appendix D.2.

When compared to re-sampling the inducing points [9], pivoted cholesky updates perform significantly better, as shown in Figure 2 on the UCI protein dataset [19]. Experimental details are given in Appendix D.2.

Application to Bayesian Optimization: In the context of BO, we condition on *hypothetical* observations, and the conditioned surrogates are discarded after each acquisition function evaluation. Since the SVGP will not be conditioned on more than a few batches of observations, we can sidestep the issue of updating inducing locations entirely by instead conditioning into an *exact GP* trained the combined pseudo-data through the pseudo-likelihood. That is, we model the data as $(\mathbf{y}, \hat{\mathbf{y}}) \sim \mathcal{N}(f, \Sigma)$ (Gaussian with block-diagonal covariance) assuming $f \sim \mathcal{GP}(\mu_\theta, k_\theta(\cdot, \cdot))$. We reach the same model by choosing \hat{X} as the inducing points in our conditioned SGPR (Section 3.1). For small n_t , an exact GP is not much slower, taking only $(n_t + p)^3$ computations instead of p^3 computations, further reduced by using low rank updates.

3.3 Local Laplace Approximations for Non-Gaussian Observations

Thus far, we have solely considered Gaussian observations. The introduction of a non-Gaussian likelihood presents a new challenge, since it implies that the current observation batch and the

⁶Alternatively, we could construct SVGPs via direct optimization of c and C .

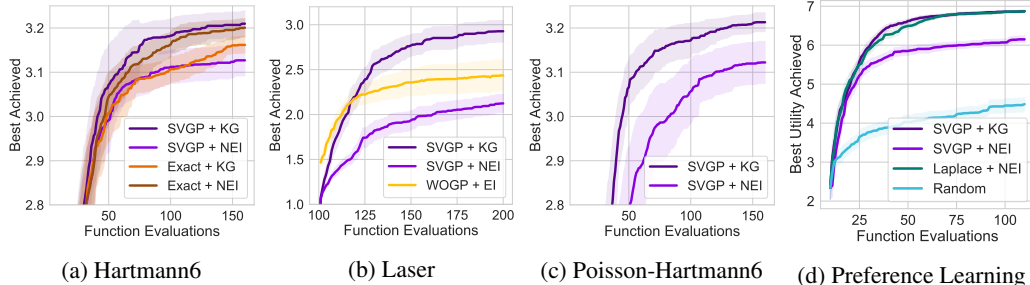


Figure 3: **(a)** Hartmann6 test problem with one constraint. Here, SVGPs with noisy expected improvement (qNEI) and KG match the performance of exact GPs with qNEI and qKG. **(b)** Free electron laser problem from McIntire et al. [51]; SVGPs with knowledge gradient outperforming weighted sparse GPs. **(c)** Constrained Hartmann6 test problem with count responses (Poisson likelihood). Only SVGPs can be used here, and qKG outperforms qNEI. **(d)** Preference learning; SVGPs with qKG are similar to Laplace approximations with NEI, and outperform qNEI with SVGPs.

pseudo-data are no longer jointly Gaussian. To adapt the conditioning procedure to the non-Gaussian setting, we can simply perform a Laplace approximation of the likelihood at the new points [65, Ch. 3]. Specifically, this gives us an approximate likelihood, $\hat{p}(y|f) = \mathcal{N}(\hat{y}; f, \mathcal{H}_*^{-1})$, where $\mathcal{H}_* = \nabla_f^2 \log p(y|f)|_{f^*(y)}$ and $f^*(y)$ is the maximizer of $\log p(y|f) + f^\top K^{-1} f$, computed via Newton iteration.⁷ When conditioning on new observations \mathbf{y} , we substitute $f^*(\mathbf{y})$ instead. That is, our new model has responses $(f^*(\mathbf{y}), \hat{\mathbf{y}})$ instead of $(\mathbf{y}, \hat{\mathbf{y}})$, and the pseudo-likelihood remains Gaussian with covariance $\Sigma = \text{blkdiag}(\mathcal{H}_*^{-1}, \Sigma_{\hat{\mathbf{y}}})$. We primarily consider natural parameterizations of one-dimensional exponential families, so that \mathcal{H}_* is positive, diagonal and depends solely on f . Computing $\nabla \log p(y|f)$ and \mathcal{H}_* is possible by hand but one can also use automatic differentiation [AD, 63].⁸ In Appendix D, Figure 8 we show the effect of repeated Laplace approximations across several batches for online classification.

4 Experiments

Our experimental evaluation demonstrates that SVGPs using OVC can be successfully used as surrogate models with advanced acquisition functions in Bayesian optimization, even in the large batch and non-Gaussian settings. In keeping with the BO literature, we will refer to the query batch size as q (not to be confused with the variational posterior $q(f)$ in previous sections). *All SVGP models that use conditioning (or fantasization) require OVC to even be practical to implement.*

Using OVC as a Building Block inside of BO

In all of our experiments, we use OVC as a *building block* to enable fantasization (Algorithm 1) within a standard BO acquisition function that requires fantasization. These acquisitions are generally “look-ahead” as a result; specifically, qKG [2, 39], LTSs, our version of qGIBBON which uses a fantasy batch [54], and qMultiStepLookAhead [39] all use the fantasization model. After adding in OVC as the `condition_on_observations` function within a BoTorch model class [2], we can simply optimize qKG or qGIBBON with an SVGP exactly as an exact GP surrogate, by using gradient based optimizers such as L-BFGS-B. In general, we need to differentiate through the fantasy model with respect to the inputs and then use gradient based methods to find the optimum. Please see Balandat et al. [2] and Frazier [24] for description of how a BO loop is constructed and how acquisition functions are optimized.

Experimental Setup In general, a Bayesian optimization loop consists of the steps of training the model and then using the trained model to optimize an acquisition function to acquire new data points,

⁷One could consider using the posterior covariance instead of K . Our experiments with the posterior covariance produced more extreme values of f and thus less regularization.

⁸Specifically, we use PyTorch’s functional API, <https://pytorch.org/docs/stable/autograd.html#functional-higher-level-api>.

which are then added into the training data for the next model. All experiments use PyTorch [62], GPyTorch [25], and BoTorch [2]. Unless otherwise specified, we run each experiment 50 times and report the mean and two standard deviations of the mean.

In the first step, we first train the inducing points, variational distribution, and kernel hyper-parameters using the evidence lower bound given in Eq. A.3. As all components are differentiable, we use the Adam optimizer with a learning rate of 0.1 and optimize for 1000 steps or until the loss converges, whichever is shorter. To initialize the inducing points, we compute a pivoted cholesky factorization on the initial kernel on the training data (described in Section 3.2 following Burt et al. [11]). The kernel hyper-parameters are initialized to GPyTorch defaults (which sets all lengthscales to one), while the variational distribution is initialized to $\mathbf{m}_u = 0$, $S_u = I$ (again, GPyTorch defaults). Further experimental details and dataset descriptions are in the Appendix.

4.1 Knowledge Gradient with SVGPs

These experiments use the one-shot formulation of the batch knowledge gradient (qKG) (Eq. 3) from Balandat et al. [2], who demonstrated that qKG outperforms other acquisitions due to being able to plan two steps into the future. *Using and optimizing qKG has only been available for exact GPs previously.* By using OVC, we have enabled SVGPs to also efficiently and tractably optimize qKG, even for non-Gaussian observations. We compare to batch noisy expected improvement [qNEI, 45] which is myopic and does not use fantasization (e.g. conditioning). Here, for the SVGPs we used $\min(N, 25)$ inducing points.

Gaussian observations: We use the **Hartmann6** test function, with one black box constraint, maximizing $f(x) = -\sum_{i=1}^4 \alpha_i \exp\{-\sum_{j=1}^6 A_{ij}(x_j - P_{ij})^2\}$ subject to the constraint that $c(x) = \|x\|_1 \leq 3$ for fixed A, P, α . We use 10 initial points and a batch size of 3 optimizing for 50 iterations, comparing to SVGPs and exact GPs using qNEI. We show the results in Figure 3a where SVGPs with qKG match exact GPs with both qNEI and qKG, and outperform SVGPs using qNEI.

Second, we mimic the **laser tuning** experiment of [51, 20], demonstrating that SVGPs outperform even weighted online GPs (WOGP), which were designed for this task. Here, we use 100 initial points, with $d = 14$, and wish to tune a laser’s output energy as a function of the magnet settings that produce the beam. Like McIntire et al. [51] we treat a pretrained GP fit on experimental data as a simulator. We use a batch size of 1, finding that SVGPs + KG outperform WOGP (Figure 3b). However, exact GPs outperform the variational approaches (Appendix Fig. 9b).

Non-Gaussian likelihoods: Next, we extend the knowledge gradient to problems with non-Gaussian likelihoods. First, we take the constrained Hartmann6 test function from the previous section, and use **Poisson** responses, $y \sim \text{Poisson}(\exp\{f(x)\})$, repeating the same settings as for the Gaussian case. Now, the data is non-Gaussian and cannot be well-modelled by a Gaussian likelihood, so we compare to only SVGPs with qNEI. qNEI is outperformed by qKG, as shown in Figure 3c.

Second, in Figure 3d, we consider a **preference learning** problem inspired by Lin et al. [46]. Here, the latent data is described by $f(x) = -10^{-1/2} \sum_{i=1}^{10} \sqrt{i} \cos(2\pi x_i)$ for $x \in [0, 1]^{10}$, comparing to Laplace approximations [15]. Again, we see that SVGPs with qKG outperform qNEI with both SVGPs and Laplace approximations.

4.2 Active Learning of Disease Incidence

We next present results for two active learning tasks governing the collection of disease incidence data. In both tasks the acquisition functions again require efficient conditioning on hypothetical data, and the second task has Binomial responses, so exact GPs cannot be applied. In both settings, applying OVC to SVGPs gives strong results competitive with either exact GPs or random forests.

Modelling of Malaria Incidence: We consider data from the Malaria Global Atlas [81] describing the infection rate of a parasite known to cause malaria in 2017. We wish to choose spatial locations to query malaria incidence in order to make the best possible predictions on a withheld test set, the entire country of Nigeria. Following Stanton et al. [70], we minimize the negative integrated posterior variance [NIPV, 68], defined as $a(\mathbf{x}; \mathcal{D}) := -\int_{\mathcal{X}} \mathbb{E}(\mathbb{V}(f(\mathbf{x})|\mathcal{D}_{+\mathbf{x}})|\mathcal{D})d\mathbf{x}$, again with $\mathcal{D}_{+\mathbf{x}} = \mathcal{D} \cup \{(\mathbf{x}, y)\}$. Intuitively, the minimizer of this acquisition will be the batch of data points that when added into the model will most reduce the total posterior uncertainty across the domain,

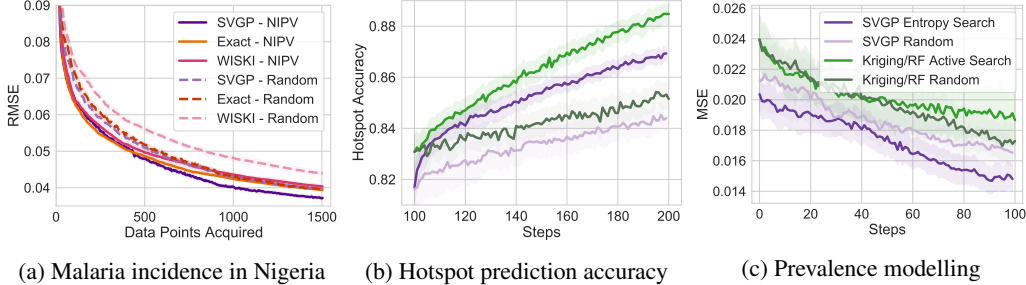


Figure 4: **(a)** Active learning of malaria incidence from satellite data. Using qNIPV outperforms randomly selecting points, while the SVGPs slightly outperform both exact GPs and WISKI. **(b,c)** Active learning of schistosomiasis incidence in Cote d’Ivoire from Andrade-Pacheco et al. [1]. Comparison is to the random forest based approach using active sampling. While the GP based models are somewhat less accurate at predicting hotspots **(b)**, they are better as a global model of prevalence **(c)**.

requiring efficient conditioning to do so in a tractable manner. The results are shown for a batch size of $q = 6$ across 15 trials in Figure 4a where we see that each method outperforms random baselines. Perhaps due to the optimization freedom, the SVGP outperforms both the exact GP and WISKI [70].

Hotspot Modelling: We follow Andrade-Pacheco et al. [1] and model the prevalence of schistosomiasis in Côte d’Ivoire using simulated responses from 1500 villages in that country, and taking into account six other demographic variables. We model the responses y (incidence) at locations \mathbf{x} with population $n(\mathbf{x})$ with a Binomial likelihood $p(y|f, \mathbf{x}) \sim \text{Binomial}(n(\mathbf{x}), r(f))$, where $r(f) = (1 + \exp\{-f\})^{-1}$. Letting $\tau \in (0, 1)$ be a threshold on the prevalence for a location to be considered a “hotspot” [1], we compute the entropy:

$$h_\tau(\mathbf{x}, \mathcal{D}) := \mathbb{E}_{p(f|\mathcal{D})}(\mathbb{H}(\text{Bernoulli}(f > \text{logit}(\tau)))) \approx \frac{1}{K} \sum_{i=1}^K \mathbb{1}_{f > \text{logit}(\tau)} \mathbb{H}(\text{Bernoulli}(f)),$$

taking the acquisition value to be the reduction in the entropy of the posterior predictive distribution over the incidence under the hotspot-focused likelihood.

$$a_\tau(\mathbf{x}, \mathcal{D}) := \int_{\mathbf{x}' \in \mathcal{X}} (h_\tau(\mathbf{x}', \mathcal{D}_{+\mathbf{x}}) - h_\tau(\mathbf{x}', \mathcal{D})) d\mathbf{x}'. \quad (9)$$

A location is given a high acquisition value if observing the incidence at that location reduces the uncertainty of the model on the predicted set of hotspots. In Figure 4b, we compare to Andrade-Pacheco et al. [1] who use spatial kriging on the residuals of a random forest model. Both their random baseline and their exploration based procedure (a variant of UCB) start off with higher prediction accuracy; however our SVGP models ultimately outperform the kriging approach with random selection. The SVGP is a better predictor of true prevalence, as shown in Figure 4c. In both cases, our acquisition function significantly outperforms random selection with a SVGP surrogate.

4.3 Rollouts within Thompson Sampling for High Dimensional BO

For our final set of experiments, we solve control problems using trust region Bayesian optimization [TurBO, 22]. Inspired by multi-step look-aheads [39, 4], we propose h -step look-ahead Thompson sampling (LTS- h). In BO, Thompson sampling (TS) is often implemented by drawing samples from the posterior at points all over the domain, then selecting the q best to form a query batch [71, 22]. LTS- h extends the idea by conditioning the surrogate independently on each posterior sample in the original TS query batch, Thompson sampling again from the updated posterior with a new set of points, and appending the best sample to its predecessor to form a *path*. The process is repeated h times. Finally, we condition the original surrogate jointly on each path, then perform TS again to choose the new query batch. Informally, each path corresponds to a distinct, coherent draw from $p(f|\mathcal{D})$, allowing the inner-loop to refine its guess of the global optimum for different f , and the final round of TS chooses the query batch based on those guesses. See Appendix C.5 for a formal description. Like other look-ahead acquisitions, LTS- h is only practical if posterior conditioning and samples are very efficient and numerically stable. LTS- h is conceptually similar to path sampling for look-ahead in Jiang et al. [39] and kriging believer [26].

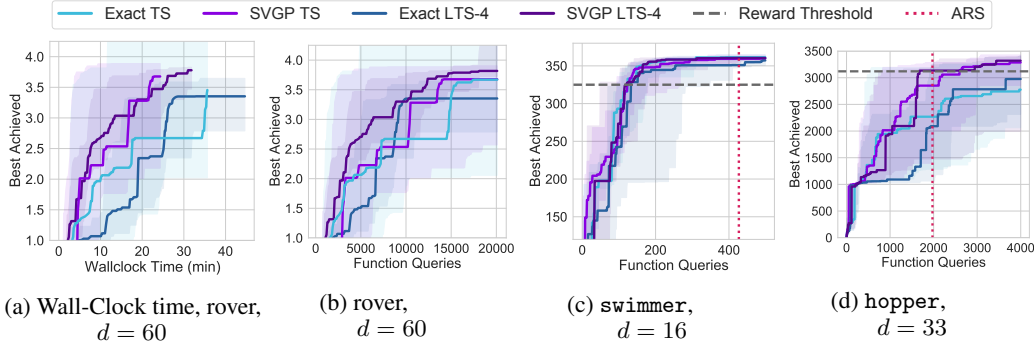


Figure 5: Multi-step rollouts with OVC and SVGPs provides sample-complexity and wall-clock time improvements on high dimensional BO problems when using TurBO and LAMCTS [22, 78]. SVGP rollouts are as time efficient (to 150 iterations) as standard TS (a) on lunar rover, $d = 60$. (c-d) MuJoCo environments using LAMCTS + TurBO. Also shown is the reward threshold (dashed grey lines) and augmented random search (ARS)’s performance (dotted red lines) [49]. The median and its 95% confidence interval are shown over 24 trials for rover and 10 trials for swimmer and hopper.

For validation, we consider tuning the 60 dimensional path that a **lunar rover** takes across a field stacked with obstacles [79, 22]. We use batches of $q = 100$ with 200 initial points, and use trust region Bayesian optimization (TurBO) to split up the space effectively [22], comparing to TurBO with Thompson sampling (TS) as the acquisition [71]. We show the wall clock times per iteration in Figure 5a, where we see that the TurBO + LTS approaches compare well in wallclock time to TurBO+TS, while being more function efficient (Figure 5b).

Finally, we consider **MuJoCo** problems using the OpenAI gym [75, 7] with LTSs inside of TurBO with trust regions generated by Monte Carlo Tree Search following the procedure of Wang et al. [78]. Following Wang et al. [78], we learn a linear policy and consider the *swimmer-v2*, *hopper-v2* environments over 10 trials displaying the median and its 95% confidence band due to high variance. On both problems, SVGP with LTSs tend to be the most sample efficient, with SVGP + TS performing at least as well on *swimmer-v2*. We also show the reward threshold and the performance achieved by augmented random search (ARS), which is a strong baseline reinforcement learning method that uses random search to tune linear controllers [49]. Our results suggest that LTSs are promising overall; however, more work needs to be done for high dimensional kernels on these problems.

5 Discussion

In conclusion, we have demonstrated how to efficiently condition on new data points with stochastic variational Gaussian processes via closed form updates to the variational distribution. Our conditioning approach generalizes exact GP conditioning via Laplace approximations for non-Gaussian likelihoods. As a result, we have decoupled look-ahead BO acquisition functions from their dependence on exact GP inference through a Gaussian likelihood, increasing the range, scale, and efficiency of BO applications. In the future, we hope to extend OVC to multi-task and deep Gaussian processes for use in Bayesian optimization [31, 17].

Acknowledgements

WJM, SS, AGW are supported by an Amazon Research Award, NSF I-DISRE 193471, NIH R01 DA048764-01A1, NSF IIS-1910266, and NSF 1922658 NRT-HDR: FUTURE Foundations, Translation, and Responsibility for Data Science. WJM was additionally supported by an NSF Graduate Research Fellowship under Grant No. DGE-1839302. SS is additionally supported by the United States Department of Defense through the National Defense Science & Engineering Graduate (NDSEG) Fellowship Program. We’d like to thank Greg Benton for setting up the volatility experiment and for helpful discussions and Nate Gruver and Eytan Bakshy for helpful comments.

References

- [1] Andrade-Pacheco, R., Rerolle, F., Lemoine, J., Hernandez, L., Meité, A., Juziwelo, L., Bibaut, A. F., van der Laan, M. J., Arnold, B. F., and Sturrock, H. J. (2020). Finding hotspots: development of an adaptive spatial sampling approach. *Scientific reports*, 10(1):1–12.
- [2] Balandat, M., Karrer, B., Jiang, D., Daulton, S., Letham, B., Wilson, A. G., and Bakshy, E. (2020). BoTorch: A Framework for Efficient Monte-Carlo Bayesian Optimization. In *Advances in Neural Information Processing Systems*, volume 33.
- [3] Bauer, M., Van Der Wilk, M., and Rasmussen, C. (2016). Understanding probabilistic sparse gaussian process approximations. In *Advances in Neural Information Processing Systems*, volume 29, pages 1533–1541.
- [4] Bertsekas, D. P. (2020). *Rollout, Policy Iteration, and Distributed Reinforcement Learning*. Athena Scientific.
- [5] Bijl, H., Schön, T. B., van Wingerden, J.-W., and Verhaegen, M. (2016). Online sparse gaussian process training with input noise. *arXiv preprint arXiv:1601.08068*.
- [6] Boedecker, J., Springenberg, J. T., Wülfing, J., and Riedmiller, M. (2014). Approximate real-time optimal control based on sparse gaussian process models. In *2014 IEEE Symposium on Adaptive Dynamic Programming and Reinforcement Learning (ADPRL)*, pages 1–8. IEEE.
- [7] Brockman, G., Cheung, V., Pettersson, L., Schneider, J., Schulman, J., Tang, J., and Zaremba, W. (2016). Openai gym. *arXiv preprint arXiv:1606.01540*.
- [8] Broderick, T., Boyd, N., Wibisono, A., Wilson, A. C., and Jordan, M. I. (2013). Streaming variational bayes. In *Advances in Neural Information Processing Systems*, volume 26.
- [9] Bui, T. D., Nguyen, C. V., and Turner, R. E. (2017a). Streaming sparse Gaussian process approximations. In *Advances in Neural Information Processing Systems*, volume 31, pages 3301–3309, Long Beach, California, USA. Curran Associates Inc.
- [10] Bui, T. D., Yan, J., and Turner, R. E. (2017b). A unifying framework for gaussian process pseudo-point approximations using power expectation propagation. *The Journal of Machine Learning Research*, 18(1):3649–3720.
- [11] Burt, D., Rasmussen, C. E., and Van Der Wilk, M. (2019). Rates of convergence for sparse variational Gaussian process regression. In *Proceedings of the 36th International Conference on Machine Learning*, volume 97, pages 862–871. PMLR.
- [12] Canu, S. and Smola, A. (2006). Kernel methods and the exponential family. *Neurocomputing*, 69(7):714–720. New Issues in Neurocomputing: 13th European Symposium on Artificial Neural Networks.
- [13] Cheng, C.-A. and Boots, B. (2016). Incremental variational sparse Gaussian process regression. In *Advances in Neural Information Processing Systems*, volume 30, pages 4410–4418, Barcelona, Spain. Curran Associates Inc.
- [14] Chowdhary, G., Kingravi, H. A., How, J. P., and Vela, P. A. (2014). Bayesian nonparametric adaptive control using gaussian processes. *IEEE transactions on neural networks and learning systems*, 26(3):537–550.
- [15] Chu, W. and Ghahramani, Z. (2005). Preference learning with gaussian processes. In *Proceedings of the 22nd International Conference on Machine learning*, pages 137–144.
- [16] Csató, L. and Opper, M. (2002). Sparse on-line gaussian processes. *Neural computation*, 14(3):641–668.
- [17] Cutajar, K., Pullin, M., Damianou, A., Lawrence, N., and González, J. (2019). Deep gaussian processes for multi-fidelity modeling. *arXiv preprint arXiv:1903.07320*.

- [18] Deisenroth, M. and Rasmussen, C. E. (2011). Pilco: A model-based and data-efficient approach to policy search. In *Proceedings of the 28th International Conference on Machine Learning*, pages 465–472.
- [19] Dua, D. and Graff, C. (2017). UCI machine learning repository.
- [20] Duris, J., Kennedy, D., Hanuka, A., Shtalenkova, J., Edelen, A., Baxevanis, P., Egger, A., Cope, T., McIntire, M., Ermon, S., et al. (2020). Bayesian optimization of a free-electron laser. *Physical review letters*, 124(12):124801.
- [21] Eriksson, D. and Jankowiak, M. (2021). High-dimensional bayesian optimization with sparse axis-aligned subspaces. *arXiv preprint arXiv:2103.00349*.
- [22] Eriksson, D., Pearce, M., Gardner, J., Turner, R. D., and Poloczek, M. (2019). Scalable global optimization via local bayesian optimization. In *Advances in Neural Information Processing Systems*, volume 32. Curran Associates, Inc.
- [23] Fine, S. and Scheinberg, K. (2001). Efficient svm training using low-rank kernel representations. *Journal of Machine Learning Research*, 2(Dec):243–264.
- [24] Frazier, P. I. (2018). A tutorial on bayesian optimization. *arXiv preprint arXiv:1807.02811*.
- [25] Gardner, J. R., Pleiss, G., Bindel, D., Weinberger, K. Q., and Wilson, A. G. (2018). GPyTorch: Blackbox Matrix-Matrix Gaussian Process Inference with GPU Acceleration. In *Advances in Neural Information Processing Systems*, volume 31.
- [26] Ginsbourger, D., Le Riche, R., and Carraro, L. (2010). Kriging is well-suited to parallelize optimization. In *Computational intelligence in expensive optimization problems*, pages 131–162. Springer.
- [27] Girard, A., Rasmussen, C. E., Candela, J. Q., and Murray-Smith, R. (2002). Gaussian process priors with uncertain inputs-application to multiple-step ahead time series forecasting. In *Advances in Neural Information Processing Systems*, volume 15.
- [28] Gómez-Bombarelli, R., Wei, J. N., Duvenaud, D., Hernández-Lobato, J. M., Sánchez-Lengeling, B., Sheberla, D., Aguilera-Iparraguirre, J., Hirzel, T. D., Adams, R. P., and Aspuru-Guzik, A. (2018). Automatic chemical design using a data-driven continuous representation of molecules. *ACS central science*, 4(2):268–276.
- [29] Groot, P., Lucas, P., and Bosch, P. (2011). Multiple-step time series forecasting with sparse gaussian processes. In *Causmaecker, P. De (ed.), Proceedings of the 23rd Benelux Conference on Artificial Intelligence*, pages 1–8. [SI: sn].
- [30] Hagan, P. S., Kumar, D., Lesniewski, A. S., and Woodward, D. E. (2002). Managing smile risk. *The Best of Wilmott*, 1:249–296.
- [31] Hebbal, A., Brevault, L., Balesdent, M., Talbi, E.-G., and Melab, N. (2021). Bayesian optimization using deep gaussian processes with applications to aerospace system design. *Optimization and Engineering*, 22(1):321–361.
- [32] Hennig, P. and Schuler, C. J. (2012). Entropy search for information-efficient global optimization. *Journal of Machine Learning Research*, 13(6).
- [33] Hensman, J., Fusi, N., and Lawrence, N. D. (2013). Gaussian processes for big data. In *Proceedings of the Twenty-Ninth Conference on Uncertainty in Artificial Intelligence, UAI'13*, page 282–290, Arlington, Virginia, USA. AUAI Press.
- [34] Hensman, J., Matthews, A., and Ghahramani, Z. (2015). Scalable Variational Gaussian Process Classification. In *Proceedings of the Eighteenth International Conference on Artificial Intelligence and Statistics*, pages 351–360, San Diego, California, USA. PMLR.
- [35] Hoang, T. N., Hoang, Q. M., and Low, B. K. H. (2015). A unifying framework of anytime sparse gaussian process regression models with stochastic variational inference for big data. In *International Conference on Machine Learning*, volume 37, pages 569–578. PMLR.

- [36] Huber, M. F. (2013). Recursive gaussian process regression. In *2013 IEEE International Conference on Acoustics, Speech and Signal Processing*, pages 3362–3366. IEEE.
- [37] Huber, M. F. (2014). Recursive gaussian process: On-line regression and learning. *Pattern Recognition Letters*, 45:85–91.
- [38] Jankowiak, M., Pleiss, G., and Gardner, J. (2020). Parametric gaussian process regressors. In *International Conference on Machine Learning*, volume 119, pages 4702–4712. PMLR.
- [39] Jiang, S., Jiang, D., Balandat, M., Karrer, B., Gardner, J., and Garnett, R. (2020). Efficient Nonmyopic Bayesian Optimization via One-Shot Multi-Step Trees. In *Advances in Neural Information Processing Systems*, volume 33.
- [40] Kapoor, S., Karaletsos, T., and Bui, T. D. (2020). Variational auto-regressive gaussian processes for continual learning. *arXiv preprint arXiv:2006.05468*.
- [41] Khan, M. and Lin, W. (2017). Conjugate-computation variational inference: Converting variational inference in non-conjugate models to inferences in conjugate models. In *Artificial Intelligence and Statistics*, pages 878–887. PMLR.
- [42] Knudde, N., van der Herten, J., Dhaene, T., and Couckuyt, I. (2017). GPflowOpt: A Bayesian Optimization Library using TensorFlow. *arXiv preprint arXiv:1711.03845*.
- [43] Krityakierne, T. and Ginsbourger, D. (2015). Global optimization with sparse and local gaussian process models. In *International Workshop on Machine Learning, Optimization and Big Data*, pages 185–196. Springer.
- [44] Lázaro-Gredilla, M., Quinonero-Candela, J., Rasmussen, C. E., and Figueiras-Vidal, A. R. (2010). Sparse spectrum gaussian process regression. *The Journal of Machine Learning Research*, 11:1865–1881.
- [45] Letham, B., Karrer, B., Ottoni, G., Bakshy, E., et al. (2019). Constrained bayesian optimization with noisy experiments. *Bayesian Analysis*, 14(2):495–519.
- [46] Lin, J., Obeng, A., and Bakshy, E. (2020). Preference learning for real-world multi-objective decision making. *ICML 2020 Workshop on Real World Experiment Design and Active Learning*.
- [47] Ling, C. K., Low, K. H., and Jaillet, P. (2016). Gaussian process planning with lipschitz continuous reward functions: Towards unifying bayesian optimization, active learning, and beyond. In *Proceedings of the AAAI Conference on Artificial Intelligence*, volume 30.
- [48] MacKenzie, D. and Spears, T. (2014). ‘the formula that killed wall street’: The gaussian copula and modelling practices in investment banking. *Social Studies of Science*, 44(3):393–417.
- [49] Mania, H., Guy, A., and Recht, B. (2018). Simple random search of static linear policies is competitive for reinforcement learning. In *Advances in Neural Information Processing Systems*, volume 31, pages 1805–1814.
- [50] Matthews, A. G. d. G. (2017). *Scalable Gaussian process inference using variational methods*. PhD thesis, University of Cambridge.
- [51] McIntire, M., Ratner, D., and Ermon, S. (2016). Sparse gaussian processes for bayesian optimization. In *Uncertainty in Artificial Intelligence*, volume 32. Association for Uncertainty in Artificial Intelligence (AUAI).
- [52] Moreno-Muñoz, P., Artés-Rodríguez, A., and Álvarez, M. A. (2019). Continual multi-task gaussian processes. *arXiv preprint arXiv:1911.00002*.
- [53] Moreno-Muñoz, P., Artés-Rodríguez, A., and Álvarez, M. A. (2020). Recyclable gaussian processes. *arXiv preprint arXiv:2010.02554*.
- [54] Moss, H. B., Leslie, D. S., Gonzalez, J., and Rayson, P. (2021). Gibbon: General-purpose information-based bayesian optimisation. *arXiv preprint arXiv:2102.03324*.

- [55] Nickson, T., Osborne, M. A., Reece, S., and Roberts, S. (2014). Automated machine learning using stochastic algorithm tuning. In *NIPS Workshop on Bayesian Optimization*.
- [56] Opper, M. (1998). A bayesian approach to online learning. *On-line learning in neural networks*, pages 363–378.
- [57] Opper, M. and Archambeau, C. (2009). The variational gaussian approximation revisited. *Neural computation*, 21(3):786–792.
- [58] Osborne, M. A. (2010). *Bayesian Gaussian processes for sequential prediction, optimisation and quadrature*. PhD thesis, Oxford University, UK.
- [59] Pan, P., Swaroop, S., Immer, A., Eschenhagen, R., Turner, R. E., and Khan, M. E. (2020). Continual deep learning by functional regularisation of memorable past. *arXiv preprint arXiv:2004.14070*.
- [60] Pan, Y., Yan, X., Theodorou, E. A., and Boots, B. (2017). Prediction under uncertainty in sparse spectrum gaussian processes with applications to filtering and control. In *International Conference on Machine Learning*, volume 70, pages 2760–2768. PMLR.
- [61] Panos, A., Dellaportas, P., and Titsias, M. K. (2018). Fully scalable gaussian processes using subspace inducing inputs. *arXiv preprint arXiv:1807.02537*.
- [62] Paszke, A., Gross, S., Massa, F., Lerer, A., Bradbury, J., Chanan, G., Killeen, T., Lin, Z., Gimelshein, N., Antiga, L., Desmaison, A., Kopf, A., Yang, E., DeVito, Z., Raison, M., Tejani, A., Chilamkurthy, S., Steiner, B., Fang, L., Bai, J., and Chintala, S. (2019). Pytorch: An imperative style, high-performance deep learning library. In *Advances in Neural Information Processing Systems*, volume 32. Curran Associates, Inc.
- [63] Pearlmutter, B. A. (1994). Fast exact multiplication by the hessian. *Neural computation*, 6(1):147–160.
- [64] Pleiss, G., Gardner, J. R., Weinberger, K. Q., and Wilson, A. G. (2018). Constant-Time Predictive Distributions for Gaussian Processes. In *Artificial Intelligence and Statistics*, volume 84. PMLR.
- [65] Rasmussen, C. E. and Williams, C. K. I. (2008). *Gaussian processes for machine learning*. Adaptive computation and machine learning. MIT Press, Cambridge, Mass., 3. print edition.
- [66] Sæmundsson, S., Hofmann, K., and Deisenroth, M. (2018). Meta reinforcement learning with latent variable gaussian processes. In *34th Conference on Uncertainty in Artificial Intelligence*, volume 34, pages 642–652. Association for Uncertainty in Artificial Intelligence (AUAI).
- [67] Seeger, M. W., Williams, C. K., and Lawrence, N. D. (2003). Fast forward selection to speed up sparse gaussian process regression. In *International Workshop on Artificial Intelligence and Statistics*, pages 254–261. PMLR.
- [68] Seo, S., Wallat, M., Graepel, T., and Obermayer, K. (2000). Gaussian process regression: Active data selection and test point rejection. In *Neural Networks, IEEE-INNS-ENNS International Joint Conference on*, volume 3, pages 3241–3241.
- [69] Shi, J., Titsias, M., and Mnih, A. (2020). Sparse orthogonal variational inference for gaussian processes. In *International Conference on Artificial Intelligence and Statistics*, volume 108, pages 1932–1942. PMLR.
- [70] Stanton, S., Maddox, W. J., Delbridge, I., and Wilson, A. G. (2021). Kernel Interpolation for Scalable Online Gaussian Processes. In *Artificial Intelligence and Statistics*, volume 130. PMLR.
- [71] Thompson, W. R. (1933). On the likelihood that one unknown probability exceeds another in view of the evidence of two samples. *Biometrika*, 25(3/4):285–294.
- [72] Titsias, M. (2008). Variational Model Selection for Sparse Gaussian Process Regression. www.aueb.gr/users/mtitsias/papers/sparseGPv2.pdf, page 20.
- [73] Titsias, M. (2009). Variational Learning of Inducing Variables in Sparse Gaussian Processes. In *Artificial Intelligence and Statistics*, pages 567–574. PMLR. ISSN: 1938-7228.

- [74] Titsias, M. K., Schwarz, J., Matthews, A. G. d. G., Pascanu, R., and Teh, Y. W. (2019). Functional regularisation for continual learning with gaussian processes. In *International Conference on Learning Representations*.
- [75] Todorov, E., Erez, T., and Tassa, Y. (2012). Mujoco: A physics engine for model-based control. In *2012 IEEE/RSJ International Conference on Intelligent Robots and Systems*, pages 5026–5033. IEEE.
- [76] Tripp, A., Daxberger, E., and Hernández-Lobato, J. M. (2020). Sample-efficient optimization in the latent space of deep generative models via weighted retraining. *Advances in Neural Information Processing Systems*, 33.
- [77] Van der Wilk, M. (2019). *Sparse Gaussian process approximations and applications*. PhD thesis, University of Cambridge.
- [78] Wang, L., Fonseca, R., and Tian, Y. (2020). Learning search space partition for black-box optimization using monte carlo tree search. In *Advances in Neural Information Processing Systems*, volume 33.
- [79] Wang, Z., Gehring, C., Kohli, P., and Jegelka, S. (2018). Batched large-scale bayesian optimization in high-dimensional spaces. In *International Conference on Artificial Intelligence and Statistics*, volume 84, pages 745–754. PMLR.
- [80] Wang, Z. and Jegelka, S. (2017). Max-value entropy search for efficient bayesian optimization. In *International Conference on Machine Learning*, volume 70, pages 3627–3635. PMLR.
- [81] Weiss, D. J., Lucas, T. C., Nguyen, M., Nandi, A. K., Bisanzio, D., Battle, K. E., Cameron, E., Twohig, K. A., Pfeffer, D. A., Rozier, J. A., et al. (2019). Mapping the global prevalence, incidence, and mortality of plasmodium falciparum, 2000–17: a spatial and temporal modelling study. *The Lancet*, 394(10195):322–331.
- [82] Wilson, A. and Ghahramani, Z. (2010). Copula Processes. In *Advances in Neural Information Processing Systems*, volume 23, page 9.
- [83] Wilson, A. and Nickisch, H. (2015). Kernel Interpolation for Scalable Structured Gaussian Processes (KISS-GP). In *International Conference on Machine Learning*, pages 1775–1784. ISSN: 1938-7228 Section: Machine Learning.
- [84] Wu, J. and Frazier, P. I. (2016). The parallel knowledge gradient method for batch Bayesian optimization. In *Advances in Neural Information Processing Systems*, volume 30 of *NIPS’16*, pages 3134–3142, Red Hook, NY, USA. Curran Associates Inc.
- [85] Xu, N., Low, K. H., Chen, J., Lim, K. K., and Ozgul, E. (2014). Gp-localize: Persistent mobile robot localization using online sparse gaussian process observation model. In *Proceedings of the AAAI Conference on Artificial Intelligence*, volume 28.

Supplementary Materials for Conditioning Sparse Variational Gaussian Processes for Online Decision-making

Table of Contents

The Appendix is structured as follows:

- Appendix A discusses broader impacts and limitations.
- Appendix B discusses the background in more detail.
- Appendix C discusses Newton’s method and training objectives for the variational models, before giving more detail on the methodological work, including implementation details.
- Appendix D shows two more understanding experiments along with ablation studies, with Appendix D.2 giving detailed experimental and data descriptions.

A Limitations and Societal Impacts

A.1 Limitations

From a practical perspective, we see several interrelated limitations:

- In our software implementation, we currently support single-output functions. This is partly because GPyTorch currently has limited support for fantasization of multi-task Gaussian processes; see <https://github.com/cornellius-gp/gpytorch/pull/805>.
- For non-Gaussian likelihoods, the approximation may break down for long rollout time steps due to accumulating error from the Laplace approximation.
- Incorrect modelling and thus incorrect rollouts will tend to be even more influential in high dimensional settings, as the kernels we use do not tend to work particularly well in high dimensions [22].
- If the underlying data is non-stationary, then long range predictions may suffer. For example, local models are superior on the rover problem in Figure 5, even compared to global models with advanced acquisition functions (e.g. Figure 12c). This limitation is remedied somewhat by the local modelling approaches we use [22, 78].
- Using many inducing points can worsen numerical conditioning, leading to less stable multi-step fantasization, despite the theoretical advantages of more inducing points [e.g., 3].

A.2 Societal Impacts

We do not anticipate that our work will have negative societal impacts. To the contrary, as we demonstrate in this paper, Bayesian optimization is naturally suited to applications in the public interest, such as public health surveillance [1]. These types of applications should help benefit global populations by allowing more targeted interventions in the public health setting. However, reliance solely on machine learning models, for example, in quantitative finance settings (as our volatility model in Figure 1c is designed for), could potentially lead to over-confidence and financial shocks as has previously been the case [48].

B Further Background

In this section, we describe further related work on both variational inference in the streaming setting as well as the use of sparse GPs in both BO and control before describing Newton’s iteration for Laplace approximations and training methods for exact and variational GPs.

B.1 Extended Related Work

Because our work explores three distinct applications, namely black-box optimization, active learning, and control, there was more noteworthy related work than the space constraints of the main text would permit. Here we present a more complete literature review.

We do not focus on other approaches for streaming variational GP inference ranging from decoupled inducing points [13, 40, 69] to alternative variational constructions [52, 53] to Kalman filtering based approaches [37, 36] to deep linear model approaches [59, 74]. These approaches could potentially be folded into OVC; however, we leave exploration of these for related work.

We also focus solely on the variationally sparse GPs introduced by Titsias [73] and Hensman et al. [33], rather than other approaches, which are potentially amenable to being used within OVC. Of particular note, the classical variational approximations for non-Gaussian likelihoods such as the approaches proposed originally by Csató and Opper [16] and later Opper and Archambeau [57] seem particularly promising, as is the development of kernel methods within the exponential family more generally [12].

From a software perspective, both GPFlowOpt [42] and its successor Trieste (<https://github.com/secondmind-labs/trieste>) seem to support variational GPs for BO but we do not know of a comprehensive benchmarking of their implementation. Implementing variational GPs for most acquisitions in BoTorch [2] is entirely possible using GPyTorch, as we did, although it requires some engineering work and is not natively supported at this time.

Recent work on molecular design has combined variational auto-encoders (VAEs) trained to map high dimensional structured molecular representations to low-dimensional latent representations with SVGPs trained to predict a molecular property of interest from the latent encoding [28, 76], but they primarily use simple acquisition functions.

In the control literature, sparse GPs are more popular, stemming from the seminal works of Csató and Opper [16] and Girard et al. [27]. Chowdhary et al. [14] directly apply the approach of Csató and Opper [16] to optimal control problems, while Ling et al. [47] sparsify GPs for active learning and planning. Groot et al. [29], Boedecker et al. [6], and Bijl et al. [5] perform multiple time step look ahead via moment matching using sparse GPs, while Pan et al. [60] use a similar approach with random fourier features. Deisenroth and Rasmussen [18] use sparse GPs to speed up dynamics models for robotics, while Sæmundsson et al. [66] use sparse GPs for meta reinforcement learning. Finally, Xu et al. [85] use sparse GPs for robot localization tasks in control.

B.2 Laplace Approximations and Newton’s Iteration

Newton iteration iterates

$$\begin{aligned} f_{t+1} &= (K^{-1} + W)^{-1}(W f_t + \nabla \log p(y|f_t)) \\ &= (K - KW^{-1/2}B^{-1}W^{-1/2}K)(W f_t + \nabla \log p(y|f_t)), \quad B := (I + W^{1/2}KW^{1/2}), \end{aligned}$$

with $W = -\nabla_f^2 \log p(y|f)$, e.g. the negative Hessian of the log likelihood, until $f_{t+1} - f_t < \epsilon$ (e.g. until a stationary point is reached). We implemented a batch version of the convergence rule, stopping when the total difference is under a threshold for all batches of f . The expensive computational cost is that of the solve of B , as W is diagonal. In our case, we only consider Newton iteration on test points, so that the time complexity is just $\mathcal{O}(n_{\text{test}}^3)$. Please see Rasmussen and Williams [Chapter 3 of 65] for further detail.

Implementation wise, for all but the GPCV experiment in Figure 1c, we manually implemented the gradient and Hessian terms as they are well known due to being natural parameterizations of exponential families. For the preference learning experiment, we followed the gradient derivation in Chu and Ghahramani [15].

B.3 Training Mechanisms for Exact Gaussian Processes and Variational Gaussian Processes

Please see the more detailed summaries of Rasmussen and Williams [65] for training methods of exact Gaussian processes as well as the theses of Van der Wilk [77] and Matthews [50] for training methods of sparse Gaussian processes. In what follows, we assume solely a zero mean function and suppress dependence on θ for the kernel matrices.

Log Marginal Likelihood for Exact GPs Training the GP’s hyper-parameters, θ , proceeds via maximizing the marginal log-likelihood (MLL). The MLL is given by

$$\log p(\mathbf{y}|X, \theta) = -\frac{1}{2}\mathbf{y}^\top(K_{\mathbf{v}\mathbf{v}} + \sigma^2 I)^{-1}\mathbf{y} - \frac{1}{2}\log|K_{\mathbf{v}\mathbf{v}} + \sigma^2 I| - \frac{n}{2}\log 2\pi, \quad (\text{A.1})$$

over the training set, $\mathcal{D} = (X, \mathbf{y})$.

Collapsed Evidence Lower Bound for SGPR Sparse Gaussian process regression (SGPR) begins by approximating the kernel with a lower rank version. The training data covariance, $K_{\mathbf{v}\mathbf{v}}$, is replaced by the Nyström approximation $K_{\mathbf{v}\mathbf{v}} \approx Q_{\mathbf{v}\mathbf{v}} := K_{\mathbf{v}\mathbf{u}}K_{\mathbf{u}\mathbf{u}}^{-1}K_{\mathbf{u}\mathbf{v}}$, where $K_{\mathbf{u}\mathbf{u}}$ is the kernel evaluated on the inducing point locations, Z . SGPR learns the locations of the inducing points and the kernel hyperparameters through a ‘collapsed’ form of the evidence lower bound (ELBO), yielding a variational adaptation of older Nyström or projected process approximations [65, Chapter 7].

The ELBO is called “collapsed” because the Gaussian likelihood allows the parameters of the variational distribution to be analytically optimized and integrated out (collapsed), yielding a bound that depends only on the inducing point locations and the kernel hyperparameters [73]. The SGPR bound is as follows (see Titsias [72] for the full derivation):

$$\mathcal{F}(\theta, Z) := \log p(y|0, \sigma^2 I + Q_{\mathbf{v}\mathbf{v}}) - \frac{1}{2\sigma^2}\text{trace}(K_{\mathbf{v}\mathbf{v}} - Q_{\mathbf{v}\mathbf{v}}). \quad (\text{A.2})$$

We can apply standard gradient based training to both the kernel hypers θ as well as the inducing locations Z . Jankowiak et al. [38] derive a variational version of this bound which enables sub-sampling across data points; we leave training with that bound for future work.

Evidence Lower Bound for SVGP The advance of Hensman et al. [33] is that they do not compute the optimal variational parameters at each time step proposing the sparse variational GP (SVGP). Their derivation, see Hensman et al. [33, 34] for a full derivation, yields an ‘uncollapsed’ ELBO (so named due to its explicit dependence on the variational parameters),

$$\mathcal{F}(\theta, Z, \mathbf{m}_{\mathbf{u}}, S_{\mathbf{u}}) := \mathbb{E}_{q(f)} \log p(y|f) - \text{KL}(\phi(\mathbf{u})||p(\mathbf{u})), \quad (\text{A.3})$$

where $q(f) = \int p(f|\mathbf{u})\phi(\mathbf{u})d\mathbf{u}$. The latent GP f is replaced with the variational distribution, $\phi(\mathbf{u}) = \mathcal{N}(\mathbf{m}_{\mathbf{u}}, S_{\mathbf{u}})$. $q(f)$ can be determined via Gaussian marginalization from $\phi(\mathbf{u})$. and is $q(f) = \mathcal{N}(K_{\mathbf{v}\mathbf{u}}K_{\mathbf{u}\mathbf{u}}^{-1}\mathbf{m}_{\mathbf{u}}, K_{\mathbf{v}\mathbf{v}} - K_{\mathbf{v}\mathbf{u}}K_{\mathbf{u}\mathbf{u}}^{-1}(K_{\mathbf{u}\mathbf{u}} - S_{\mathbf{u}})K_{\mathbf{u}\mathbf{u}}^{-1}K_{\mathbf{u}\mathbf{v}})$. Mini-batching is possible because the first term in Eq. A.3 splits over each of the n data points as each y_i is conditionally independent given f , allowing sub-sampling. Sub-sampling and mini-batching enable the use of stochastic optimization techniques, reducing the per iteration cost to be constant in n , the number of data points.

Bui et al. [9] introduce a streaming version of the ELBO that involves two further terms; the method is called O-SVGP. Their primary model, O-SGPR (called the “collapsed bound” of a streaming sparse GP in that paper) is trained through a variant of their ELBO bound that integrates out the variational parameters. We describe this collapsed bound in more detail in Appendix C.4.

Predictive Log Likelihood for SVGP We close this section by quickly describing the predictive log likelihood (PLL) method of Jankowiak et al. [38], which is motivated by attempting to improve the calibration of SVGP models trained via the ELBO. The key advance in Jankowiak et al. [38] is that they consider the expectation over both the data and the response, rather than simply the expectation over the response in the variational distribution, producing an objective that becomes:

$$\begin{aligned} \mathcal{F}(\theta, x_m, \mathbf{m}_{\mathbf{u}}, S_{\mathbf{u}}) &:= \mathbb{E}_{p(y,x)} \log p(y|f, x) - \text{KL}(\phi(\mathbf{u})||p(\mathbf{u})) \\ &\approx \sum_{i=1}^N \log (\mathbb{E}_{\phi(\mathbf{u})p(f_i|\mathbf{u}, x_i)} p(y_i|f_i)) - \text{KL}(\phi(\mathbf{u})||p(\mathbf{u})). \end{aligned}$$

We consider this optimization objective for several of the larger-scale problems here.

C Further Methodological Details

In this Appendix, we begin by presenting our approach, OVC, as a generalization of exact Gaussian conditioning for SGPR (C.1) before describing an alternative interpretation of Bui et al. [9] that is equivalent to our approach in C.2. Then, in Appendix C.3, we describe the practical implementation of OVC. In C.4, we describe a flaw of the O-SGPR bound for small batch sizes. Finally, in C.5, we give an extended description of look-ahead Thompson sampling (LTS).

C.1 OVC Generalizes Efficient Batch SGPR Conditioning

In this section, we show that OVC can also be viewed as a generalization of Gaussian conditioning for SGPR. Gaussian conditioning for SGPR is recovered as a special case of OVC when $\theta' = \theta$ and $Z' = Z$. Under this assumption, Eqns. (6) and (7) simplify as follows:

$$\mathbf{c} = K_{\mathbf{uv}}\Sigma_{\mathbf{y}}^{-1}\mathbf{y} + \mathbf{c}', \quad C = K_{\mathbf{uv}}\Sigma_{\mathbf{y}}^{-1}K_{\mathbf{vu}} + C'. \quad (\text{A.4})$$

Considering the predictive distribution given by Eq. 2 in the main text, as we add new data points, $(X_{\text{batch}}, \mathbf{y})$, into the model, we need to update $A = (K_{\mathbf{uu}} + C)^{-1}$, $\mathbf{a} = A\mathbf{c}$, and $R = (K_{\mathbf{uu}}^{-1} - A)^{1/2}$. For homoscedastic likelihoods the A update is a fast low-rank update via the Woodbury matrix identity,

$$A = A' - A'K_{\mathbf{uv}}(\sigma^2 I + K_{\mathbf{vu}}A'K_{\mathbf{uv}})^{-1}K_{\mathbf{vu}}A'. \quad (\text{A.5})$$

This produces efficient Sherman-Morrison updates to generate \mathbf{a} (via addition and matrix vector multiplication) and Woodbury based updates to update R , the predictive covariance cache via low-rank updates (e.g. Proposition 2 of Jiang et al. [39]).

Furthermore, these low rank updates can be used to produce updates to the exact caches. These updates are simply exact Gaussian conditioning with an approximate kernel. That is, the SGPR caches are merely transformed exact caches for any given set of data points. To demonstrate, we use a Nyström approximation for the kernel throughout, e.g. $K_{\mathbf{vw}} \approx K_{\mathbf{vu}}K_{\mathbf{uu}}^{-1}K_{\mathbf{uw}}$, then after applying Woodbury we can write the exact caches using A :

$$\begin{aligned} RR^\top &= (K_{\mathbf{vv}} + \Sigma_{\mathbf{y}})^{-1} = \Sigma_{\mathbf{y}}^{-1} - \Sigma_{\mathbf{y}}^{-1}K_{\mathbf{vu}}(K_{\mathbf{uu}} + K_{\mathbf{uv}}\Sigma_{\mathbf{y}}^{-1}K_{\mathbf{vu}})^{-1}K_{\mathbf{uv}}\Sigma_{\mathbf{y}}^{-1} \\ &= \Sigma_{\mathbf{y}}^{-1} - \Sigma_{\mathbf{y}}^{-1}K_{\mathbf{vu}}AK_{\mathbf{uv}}\Sigma_{\mathbf{y}}^{-1} \end{aligned}$$

with a similar expression for the predictive mean cache as

$$\mathbf{a} = (K_{\mathbf{vv}} + \Sigma_{\mathbf{y}})^{-1}\mathbf{y} = \Sigma_{\mathbf{y}}^{-1}\mathbf{y} - \Sigma_{\mathbf{y}}^{-1}K_{\mathbf{vu}}A\mathbf{c}.$$

Next we take the caches computed on every training point and project them into the space of inducing points by multiplying them by $K_{\mathbf{uu}}^{-1}K_{\mathbf{uv}}$. It takes a bit of algebra, but we can derive updated expressions for RR^\top and \mathbf{a} in terms of solely the new covariance matrix, $K_{\mathbf{vu}}$ and the new responses, $\Sigma_{\mathbf{y}}^{-1}\mathbf{y}$. That is, $\mathbf{a}_{\text{SGPR}} = K_{\mathbf{uu}}^{-1}K_{\mathbf{uv}}\mathbf{a}$ and $RR_{\text{SGPR}}^\top = K_{\mathbf{uu}}^{-1}K_{\mathbf{uv}}RR^\top K_{\mathbf{vu}}K_{\mathbf{uu}}^{-1}$.

$$\begin{aligned} \mathbf{a}_{\text{SGPR}} &= K_{\mathbf{uu}}^{-1}K_{\mathbf{uv}}(\Sigma_{\mathbf{y}}^{-1}\mathbf{y} - \Sigma_{\mathbf{y}}^{-1}K_{\mathbf{vu}}AK_{\mathbf{uv}}\Sigma_{\mathbf{y}}^{-1}\mathbf{y}) = K_{\mathbf{uu}}^{-1}\mathbf{c} - K_{\mathbf{uu}}^{-1}C(K_{\mathbf{uu}} + C)^{-1}\mathbf{c} \\ &= K_{\mathbf{uu}}^{-1}((K_{\mathbf{uu}} + C)(K_{\mathbf{uu}} + C)^{-1} - C(K_{\mathbf{uu}} + C)^{-1})\mathbf{c} = (K_{\mathbf{uu}} + C)^{-1}\mathbf{c} \end{aligned}$$

and similarly

$$\begin{aligned} RR_{\text{SGPR}}^\top &= K_{\mathbf{uu}}^{-1}K_{\mathbf{uv}}RR^\top K_{\mathbf{vu}}K_{\mathbf{uu}}^{-1} = K_{\mathbf{uu}}^{-1}K_{\mathbf{uv}}(\Sigma_{\mathbf{y}}^{-1} - \Sigma_{\mathbf{y}}^{-1}K_{\mathbf{vu}}AK_{\mathbf{uv}}\Sigma_{\mathbf{y}}^{-1})K_{\mathbf{vu}}K_{\mathbf{uu}}^{-1} \\ &= K_{\mathbf{uu}}^{-1}K_{\mathbf{uu}} - K_{\mathbf{uu}}^{-1}CACK_{\mathbf{uu}}^{-1} = K_{\mathbf{uu}}^{-1}(K_{\mathbf{uu}}(K_{\mathbf{uu}} + C)^{-1}CK_{\mathbf{uu}}^{-1}) \\ &= (K_{\mathbf{uu}} + C)^{-1}CK_{\mathbf{uu}}^{-1} = (K_{\mathbf{uu}} + K_{\mathbf{uu}}C^{-1}K_{\mathbf{uu}})^{-1} \\ &= K_{\mathbf{uu}}^{-1} - (K_{\mathbf{uu}} + C)^{-1}. \end{aligned}$$

Similarly one could follow this logic in reverse to go from SGPR caching to caching for exact GP inference. We can also use the updates in Eq. A.4 to update the exact GPs caches via first updating the SGPR caches.

To summarize, exact GP regression is just Gaussian conditioning, which can be viewed as a special case of SGPR if one inducing point is placed at every data point. SGPR in turn is again Gaussian conditioning through an approximate kernel on projected features, which can be viewed as a special case of O-SGPR if the inducing points and kernel hyperparameters are held fixed. Finally O-SGPR can be viewed as a special case of O-SVGP if the variational parameters are constrained to be optimal.

C.2 Interpreting Bui et al. [9] as O-SGPR

The approach outlined in Section 3.1 can be verified to be equivalent to streaming sparse GPs (e.g. the un-collapsed bound of Bui et al. [9]) mechanically by verifying that the expressions for the ELBO are equivalent (up to constants) and that the predictive mean and variance are exactly equivalent. Although verifying the equivalence is simply a matter of manipulating algebraic expressions, we have not yet justified the choice of $\hat{\mathbf{y}}$ and $\Sigma_{\hat{\mathbf{y}}}$. Bui et al. [9] obtained their expressions by means of variational calculus, and arrived at the correct result, but did not provide much in the way of intuition for the nature of the optimal solution.

We now show how the choice of pseudo-targets $\hat{\mathbf{y}}$ and pseudo-likelihood covariance $\Sigma_{\hat{\mathbf{y}}}$ has a clear interpretation that obviates any need to appeal to variational calculus except as a formal guarantee of optimality. Again, suppose we are given a sparse variational GP with inducing points Z' , kernel hyperparameters θ' and a pre-computed optimal variational distribution $\phi(\mathbf{u}') = \mathcal{N}(\mathbf{m}_{\mathbf{u}'}, S_{\mathbf{u}'})$, and then asked to find the likelihood and dataset of size p that produced the model. Although the problem as stated is under-determined, if we choose $X = Z'$ and assume the likelihood is some Gaussian centered at f , then we can reverse Eqn. (5) (in the main text) to solve for \mathbf{y} and $\Sigma_{\mathbf{y}}$ as follows:

$$\begin{aligned} \mathbf{m}_{\mathbf{u}'} &= K'_{\mathbf{u}'\mathbf{u}'}(K'_{\mathbf{u}'\mathbf{u}'} + K'_{\mathbf{u}'\mathbf{u}'}\Sigma_{\mathbf{y}}K'_{\mathbf{u}'\mathbf{u}'})^{-1}K'_{\mathbf{u}'\mathbf{u}'}\Sigma_{\mathbf{y}}^{-1}\mathbf{y}, \\ &\Rightarrow \mathbf{y} = (\Sigma_{\mathbf{y}}K'^{-1}_{\mathbf{u}'\mathbf{u}'} + I)\mathbf{m}_{\mathbf{u}'} = \hat{\mathbf{y}} \end{aligned} \quad (\text{A.6})$$

$$\begin{aligned} S_{\mathbf{u}'} &= K'_{\mathbf{u}'\mathbf{u}'}(K'_{\mathbf{u}'\mathbf{u}'} + K'_{\mathbf{u}'\mathbf{u}'}\Sigma_{\mathbf{y}}K'_{\mathbf{u}'\mathbf{u}'})^{-1}K'_{\mathbf{u}'\mathbf{u}'}, \\ &\Rightarrow \Sigma_{\mathbf{y}} = (S_{\mathbf{u}'}^{-1} - K'^{-1}_{\mathbf{u}'\mathbf{u}'})^{-1} = \Sigma_{\hat{\mathbf{y}}}. \end{aligned} \quad (\text{A.7})$$

As a result, we can now provide new, intuitive interpretations of $\hat{\mathbf{y}}$, $\Sigma_{\hat{\mathbf{y}}}$ and $\phi(\mathbf{u})$. In simple terms, the streaming sparse GP (i.e. O-SGPR) of Bui et al. [9] is equivalent to a sequence of SGPR models, where instead of training on all previously observed data through the original likelihood at each timestep, each model trains *only* on the combination of the current batch of data ($X_{\text{batch}}, \mathbf{y}$), and the pseudo-data ($Z', \hat{\mathbf{y}}$) through a pseudo-likelihood with covariance $\Sigma = \text{blkdiag}(\Sigma_{\hat{\mathbf{y}}}, \Sigma_{\mathbf{y}})$. The pseudo-data and pseudo-likelihood together represent all the past data and models. Furthermore, $(Z', \hat{\mathbf{y}})$ and $\Sigma_{\hat{\mathbf{y}}}$ are the *unique* size- m dataset with $X = Z'$ and f -centered Gaussian likelihood that could have produced $\phi(\mathbf{u}')$, given Z' and θ' . In other words we can think of the tuple $(\theta', Z', \hat{\mathbf{y}}, \Sigma_{\hat{\mathbf{y}}})$ as a compressed representation of the sparse GP it defines.

C.3 Practical Implementation

Implementation wise and to reduce our engineering overhead, we focused on computing $\hat{\mathbf{y}}$ and $\Sigma_{\hat{\mathbf{y}}}$ in a numerically stable manner. We start with the pseudo-covariance term, which can be simplified as

$$\Sigma_{\hat{\mathbf{y}}} = I + S_{\mathbf{u}'}(K'_{\mathbf{u}'\mathbf{u}'} - S_{\mathbf{u}'})^{-1}S_{\mathbf{u}'}$$

After some more algebra, we can rewrite the pseudo-observations that depend on the inducing points,

$$\begin{aligned} \hat{\mathbf{y}} &= \Sigma_{\hat{\mathbf{y}}}S_{\mathbf{u}'}^{-1}\mathbf{m}_{\mathbf{u}'} = (I + S_{\mathbf{u}'}(K'_{\mathbf{u}'\mathbf{u}'} - S_{\mathbf{u}'})^{-1}S_{\mathbf{u}'})S_{\mathbf{u}'}^{-1}\mathbf{m}_{\mathbf{u}'} \\ &= S_{\mathbf{u}'}^{-1}\mathbf{m}_{\mathbf{u}'} + S_{\mathbf{u}'}(K'_{\mathbf{u}'\mathbf{u}'} - S_{\mathbf{u}'})^{-1}\mathbf{m}_{\mathbf{u}'} \end{aligned} \quad (\text{A.8})$$

For numerical stability, we replace inverses of matrix subtractions as $((K - S)^{-1}(K - S)^{-\top})(K - S)^{\top}$, dropping subscripts. While there is still a matrix subtraction here, squaring the system improves the numerical stability of the systems, as we are forcing all of the eigenvalues of the matrices that we are solving linear systems with to be non-negative.

In practice however, we use "whitening" of the variational distribution as introduced by [50]. We instead optimize $\tilde{\mathbf{m}}_{\mathbf{u}} = K_{\mathbf{u}\mathbf{u}}^{-1/2}\mathbf{m}_{\mathbf{u}}$ and $\tilde{S}_{\mathbf{u}} = K_{\mathbf{u}\mathbf{u}}^{-1/2}S_{\mathbf{u}}K_{\mathbf{u}\mathbf{u}}^{-1/2}$. We can rewrite $\Sigma_{\hat{\mathbf{y}}}$ using the whitened variational covariance matrix $\tilde{S}_{\mathbf{u}'}$ producing, $\Sigma_{\hat{\mathbf{y}}} = K_{\mathbf{u}'\mathbf{u}'}^{1/2}(\tilde{S}_{\mathbf{u}'} + \tilde{S}_{\mathbf{u}'}(I - \tilde{S}_{\mathbf{u}'})^{-1}\tilde{S}_{\mathbf{u}'})K_{\mathbf{u}'\mathbf{u}'}^{1/2}$. Again, we square the second term to enhance stability, although it already has a symmetric form; that is, we compute

$$\Sigma_{\hat{\mathbf{y}}} = K_{\mathbf{u}'\mathbf{u}'}^{1/2}(\tilde{S}_{\mathbf{u}'} + \tilde{S}_{\mathbf{u}'}(I - \tilde{S}_{\mathbf{u}'})^{-1}(I - \tilde{S}_{\mathbf{u}'})^{-\top}(I - \tilde{S}_{\mathbf{u}'})^{\top}\tilde{S}_{\mathbf{u}'})K_{\mathbf{u}'\mathbf{u}'}^{1/2}$$

Similarly, Eq. A.7 simplifies to become

$$\hat{\mathbf{y}} = K_{\mathbf{u}'\mathbf{u}'}^{1/2}(I - \tilde{S}_{\mathbf{u}'})^{-1}\tilde{\mathbf{m}}_{\mathbf{u}'} = K_{\mathbf{u}'\mathbf{u}'}^{1/2}(I - \tilde{S}_{\mathbf{u}'})^{-1}(I - \tilde{S}_{\mathbf{u}'})^{-\top}(I - \tilde{S}_{\mathbf{u}'})^{\top}\tilde{\mathbf{m}}_{\mathbf{u}'}$$

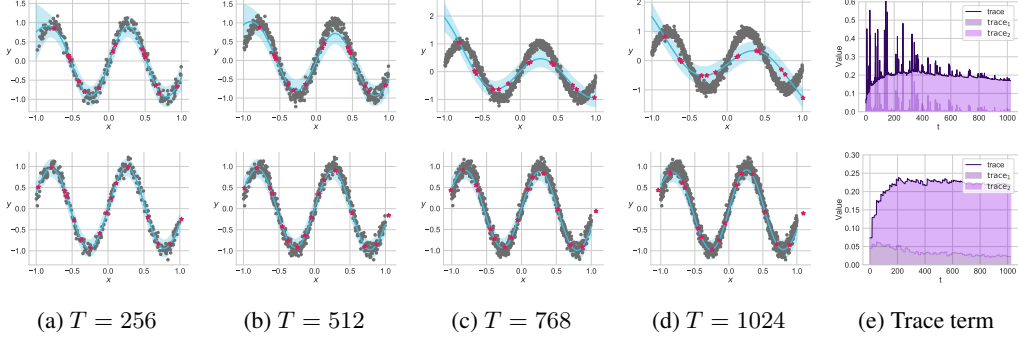


Figure 6: O-SGPR ($p = 16$) learning on i.i.d. observations without re-sampling the inducing points from a noisy sine function. **Top row:** As the number of data points increases for a batch size of 1, the model progressively underfits due to excess regularization. The trace term is entirely dominated by trace_2 . **Bottom row:** For a larger batch size ($b = 16$), there is no under-fitting and trace_1 takes up more of the overall trace term.

From an engineering point of view, as we condition into an exact GP for most of our applications, we are able to use the pseudo-likelihood covariance alongside the cache of the pseudo-data covariance, caching a root decomposition of the matrix $(K_{\text{joint}} + \text{blkdiag}(\Sigma_{\hat{y}}, \Sigma_{\mathbf{y}}))^{-1}$ via low-rank updates to a pre-existing root decomposition of $K_{\mathbf{uu}} + \Sigma_{\hat{y}}$ (and its inverse), where $K_{\text{joint}} = k_{\theta}(\text{cat}(Z, X_{\text{batch}}), \text{cat}(Z, X_{\text{batch}}))$ [64, 39]. On performing several steps of conditioning (e.g. rollouts), we then use exact GP conditioning via low rank updates as implemented in GPyTorch (which uses the strategy of Jiang et al. [39] internally) after the first step.

C.4 Incremental O-SGPR Tends to Underfit the Data

In this section we discuss a pathology of the ELBO derived in Bui et al. [9] that occurs when O-SGPR is updated on very small batches on new data (e.g. 1 new observation). Tellingly, Bui et al. [9] only considered tasks with large batch sizes (around 100 new observations per batch in each task).

Bui et al. [9] propose a “collapsed” evidence lower bound to train their O-SGPR model for each new batch of data. It is written as:

$$\begin{aligned} \mathcal{F}_{\text{OSGPR}}(\theta, \mathbf{u}) &= \log \mathcal{N}(\text{cat}(\hat{\mathbf{y}}, \mathbf{y}) | \mathbf{0}, Q_{\text{joint}} + \text{blkdiag}(\Sigma_{\hat{y}}, \Sigma_{\mathbf{y}})) \\ &\quad - \frac{1}{2}(\text{trace}_1 + \text{trace}_2) + \text{constants}, \end{aligned} \quad (\text{A.9})$$

$$\begin{aligned} \text{trace}_1 &= \sigma^{-2} \text{Tr}(K_{\mathbf{vv}} - K_{\mathbf{vu}} K_{\mathbf{uu}}^{-1} K_{\mathbf{uv}}), \\ \text{trace}_2 &= \text{Tr}((S_{\mathbf{u}'}^{-1} - K_{\mathbf{u}'\mathbf{u}'}^{-1})(K_{\mathbf{u}'\mathbf{u}'} - K_{\mathbf{u}'\mathbf{u}} K_{\mathbf{uu}}^{-1} K_{\mathbf{uu}'})), \end{aligned}$$

where $Q_{\text{joint}} = [K_{\mathbf{uu}}, K_{\mathbf{uv}}]^{\top} K_{\mathbf{uu}}^{-1} [K_{\mathbf{uu}}, K_{\mathbf{uv}}]$, and constants is composed of terms that do not depend on θ or Z . In a close parallel to the observations of Titsias [73] (e.g. Eq. A.2), we see that the O-SGPR objective is composed of a likelihood term and a trace term (written as $\text{trace}_1 + \text{trace}_2$), the latter acting as a regularizer [73, 3]. The first part of the trace term, trace_1 , has the same interpretation as the trace term in the batch setting – it is minimized when the Nystrom approximation of the kernel matrix at X_{batch} is exact (i.e. $K_{\mathbf{vv}} = K_{\mathbf{vu}} K_{\mathbf{uu}}^{-1} K_{\mathbf{uv}}$). The second trace term, trace_2 , is minimized when $Z' = Z$, so it regularizes the new inducing point locations to be close to the old locations. If the batch size, b , is much less than p then the trace term is dominated by trace_2 , which is after all a sum over p terms, compared to trace_1 which is a sum over b terms. Since the loss encourages the model to keep Z' close to Z to minimize trace_2 , the model can simply increase σ^2 to also decrease trace_1 to explain new observations by under-fitting. An analogous problem for small batch sizes was described in the Appendix of Stanton et al. [70] for the un-collapsed bound (e.g. the training procedure of an O-SVGP model) of Bui et al. [9], necessitating Stanton et al. [70] to propose a variant that down-weights the prior terms in the objective. The cost of down-weighting is an increased tendency towards over-fitting as well as an additional hyper-parameter, both of which were observed by Stanton et al. [70].

Algorithm 2 LTS with SVGP

Input: Observed data $\mathcal{D} = (X, \mathbf{y})$; SVGP model, \mathcal{M} ; candidate set generation utility, $C_{\text{gen}}()$, rollout steps, T , parallel path parameter l , top k parameter, q batch size.

Output: Candidates for evaluation $\tilde{\mathbf{X}}_{\text{end}}$.

1. Generate initial candidate set, $X_1 = C_{\text{gen}}()$.
 2. Compute posterior over candidate set, drawing a posterior sample: $y_1 \sim p(y|X_1, \mathcal{M})$.
 3. Sort y_1 and keep top l samples \tilde{y}_0 and corresponding candidates, \tilde{X}_1 .
 4. Generate $\mathcal{M}_1 \leftarrow \text{OVC}(\mathcal{M}, (\tilde{X}_1, \tilde{y}_0).\text{unsqueeze}(-1))$ via Algorithm 1. \mathcal{M}_1 is a batch of l models each conditioned on a single data point.
 - for** t in $2:T$ **do**
 5. Generate initial candidate set, $X_t = C_{\text{gen}}()$.
 6. Compute posterior over candidate set, drawing a posterior sample: $y_t \sim p(y|X_t, \mathcal{M}_{t-1})$.
 7. Sort y_t and keep top l samples \tilde{y}_t and corresponding candidates, \tilde{X}_t .
 8. Generate $\mathcal{M}_t \leftarrow \text{OVC}(\mathcal{M}_{t-1}, (\tilde{X}_t, \tilde{y}_t))$ using Algorithm 1.
 - end for**
 9. Generate $\mathcal{M}_{\text{end}} \leftarrow \text{OVC}(\mathcal{M}, (\tilde{X}_i, \tilde{y}_i)_{i=1}^T)$ using Algorithm 1.
 - Generate final candidate set, $X_{\text{end}} = C_{\text{gen}}()$.
 10. Compute posterior over candidate set, drawing a posterior sample: $y_{\text{end}} \sim p(y|X_{\text{end}}, \mathcal{M})$.
 11. Sort y_{end} and return top q corresponding candidates, $\tilde{\mathbf{X}}_{\text{end}}$.
-

In Figure 6, we empirically demonstrate the pathology of the O-SGPR bound with small batch sizes in the i.i.d. setting. In the top row, we add $b = 1$ data point at a time while continuing to re-train. Although the O-SGPR model originally fits the data well at $T = 256$, it progressively begins underfitting, which becomes more and more noticeable, especially by $T = 1024$. By comparison, a larger batch size, $b = 16$, prevents any under-fitting from occurring. In the far right panel, we see the two terms in the trace component; in the small batch setting, the inducing trace term dominates the total trace. The effect is mediated by a larger batch size, as shown in the bottom right panel.

Informally, if the number of old inducing points is much greater than the number of new observations, then O-SGPR will focus on replicating the old variational distribution. Note that either aggregating multiple batches for each update or conditioning O-SGPR into an exact GP remedies the issue.

C.5 Look-Ahead Thompson Sampling

Thompson sampling in continuous domains: in the context of black-box optimization, the action space is simply the input space, \mathcal{X} , since we are deciding which input $\mathbf{x} \in \mathcal{X}$ we will query next. Thompson sampling draws the next query point from the Bayes-optimal distribution over the possible choices, $\mathbf{x}^* \sim p_{\text{TS}}(\mathbf{x})$, where

$$p_{\text{TS}}(\mathbf{x}) \propto \int \mathbb{1}\{f(\mathbf{x}) = \sup_{\mathbf{x}' \in \mathcal{X}} f(\mathbf{x}')\} p(f|\mathcal{D}) df. \quad (\text{A.10})$$

When \mathcal{X} is a continuous domain, as is usually the case, we replace the $\sup_{\mathbf{x}' \in \mathcal{X}}$ with a $\max_{\mathbf{x}' \in X_{\text{cand}}}$, where $X_{\text{cand}} \subset \mathcal{X}$. As the name suggests, rather than attempting to evaluate the integral in Eq. (A.10), Thompson sampling instead draws samples $f_i \sim p(f|\mathcal{D})$, $i \in \{1, \dots, q\}$ and take $\mathbf{x}_i^* = \text{argmax}_{\mathbf{x}' \in X_{\text{cand}}} f_i(\mathbf{x}')$.

The look-ahead case: If we were able to evaluate each f_i on every point $\mathbf{x} \in \mathcal{X}$ and compute $\sup_{\mathbf{x}' \in \mathcal{X}} f_i(\mathbf{x}')$ exactly, there would be no benefit to multiple rounds of Thompson sampling. However, as we noted above, typically we rely on a max over a discrete set X_{cand} , typically obtained from a (quasi-)Monte Carlo method (e.g. Sobol sequences) to cover \mathcal{X} , and the number of candidate points is restricted by compute and memory. Therefore we can do multiple rounds of Thompson sampling to try to refine the estimate of \mathbf{x}_i^* by evaluating $\text{argmax}_{\mathbf{x}' \in X_j} f_i(\mathbf{x}')$ for a sequence of candidate sets X_j , $j \in \{0, \dots, h\}$. The key challenge with GPs is to ensure that f_i is consistent across the sequence of candidate sets, which we accomplish by drawing $f_i(\mathbf{x}') \sim p(f|\mathcal{D} \cup \{(\mathbf{x}_{j-1}^*, f_i(\mathbf{x}_{j-1}^*)\})$ for $\mathbf{x}' \in X_j$ and $j > 0$. The result is again $\mathbf{x}_i^* = \max_{\mathbf{x}' \in X_{\text{cand}}} f_i(\mathbf{x}')$, but now $X_{\text{cand}} = \bigcup_j X_j$.

In Algorithm 2, we describe how OVC is used within LTSs as an example of its usecase. Here, of course, we are only performing Thompson sampling over a discrete set of values and so do not end up needing to use gradient based acquisitions. Specifically, we continue using OVC (or really after $T = 1$, exact GP conditioning with low-rank updates [39] as the GP is now exact), to condition our model on each step’s fantasy responses \tilde{y}_t and the observations \tilde{X}_{batch} .

D Further Experimental Details and Results

D.1 Updating O-SGPR Inducing Points

We illustrate the efficacy of this choice of new inducing points in Figure 7 using the same time series data as in Stanton et al. [70] originally from <https://raw.githubusercontent.com/trungngv/cogp/master/data/fx/fx2007-processed.csv> (that repo uses BSD License). Re-sampling the old inducing points is shown in the top row, and tends to first perform well, but then begins to catastrophically forget by $t = 40$ and dramatically so by $t = 60$, as all of the inducing points have moved over to the right. By comparison, our approach of iteratively running a pivoted cholesky on the current inducing points and the new data point, prevents catastrophic forgetting, while also enabling the model to learn on the new data stream.

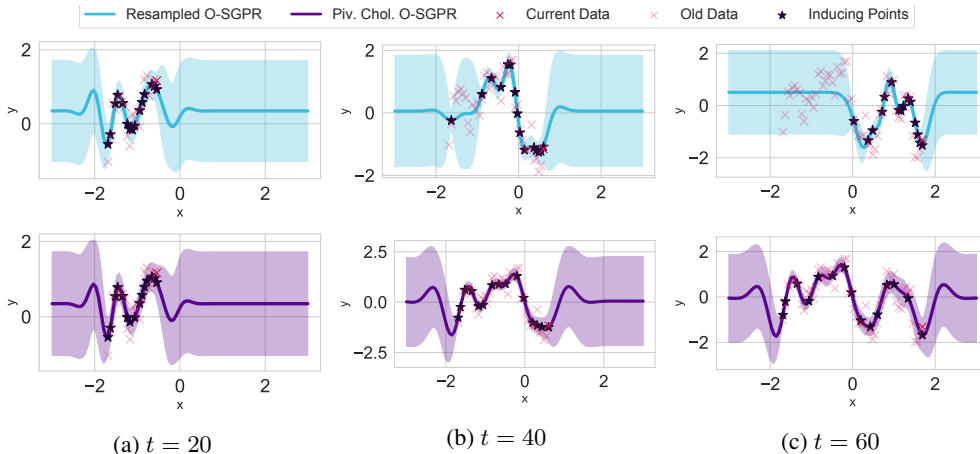


Figure 7: Online SVGP modelling a time series **Top row:** inducing points are updated by replacing an inducing point with the new location as in Bui et al. [9]. **Bottom row:** Inducing points are updated by re-running a pivoted cholesky on both the new data point and the current inducing points. The recursive refitting procedure of the pivoted cholesky placement remedies the catastrophic overfitting and forgetting of merely resampling the inducing points.

In Figure 8, we illustrate the effect of Laplace approximations during a rollout following the streaming classification example of Bui et al. [9] as we use OVC. We first trained a SVGP model with 25 inducing points on 100 data points, as shown in the first rows, then performed three steps of rollouts each with 100 data points each as we observe progressively more and more of the dataset. In the middle row, we show the predicted probability on a held-out test set; as we observe more data, the predictions become more and more confident throughout the entire region, and are un-confident in the regions where we have not observed any data. This effect is similarly observed by the predictive variances, which are high in regions where we have not seen any data, but decay as we observe each region successively. Data from https://github.com/thangbui/streaming_sparse_gp/tree/master/data (Apache 2.0 License).

D.2 Experimental and Data Details

Unless otherwise specified, all data is simulated. The code primarily relies on PyTorch [62] (MIT License), BoTorch [2] (MIT License), GPyTorch [25] (MIT License). All GPs (variational and exact) used a constant mean, scaled Matern-5/2 kernels with ARD with lengthscale priors of $\text{Gamma}(3, 6)$ and outputscale priors of $\text{Gamma}(2, 0.15)$, which are the current BoTorch defaults for single task GPs.

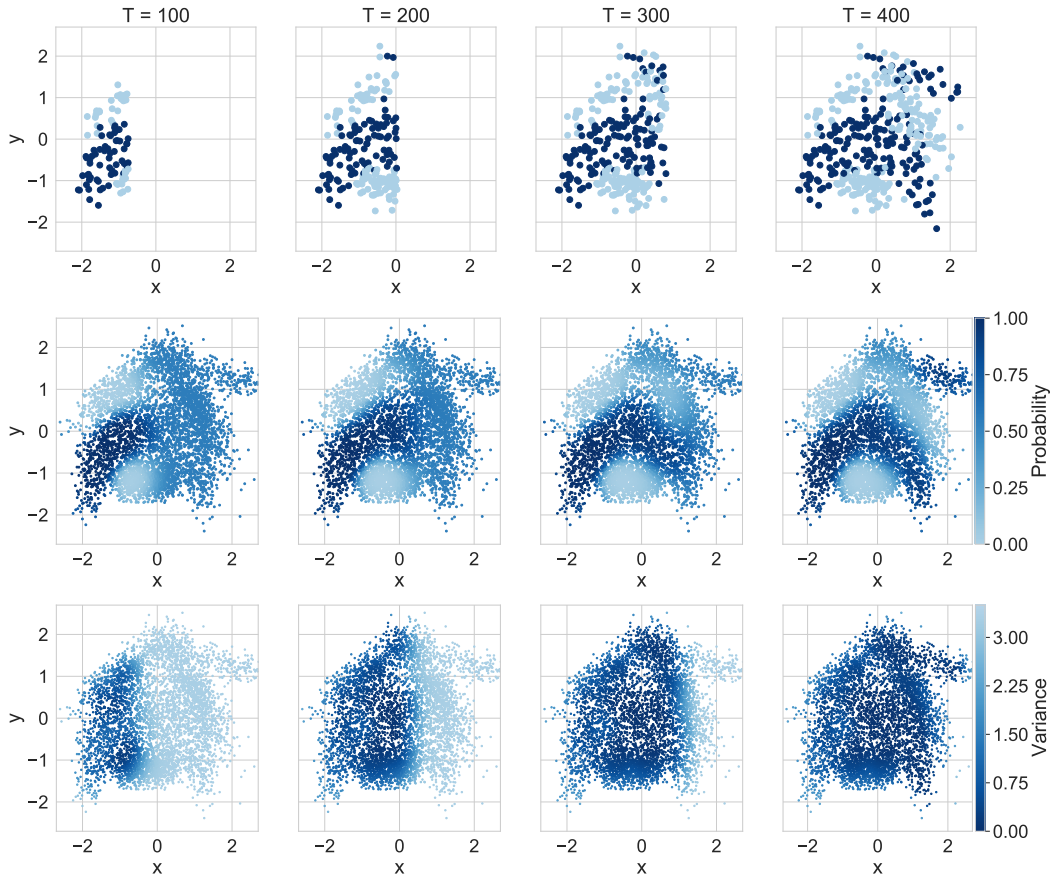


Figure 8: **Top row:** Data from the bananas dataset arriving in a non-i.i.d fashion in four successive batches. **Middle row:** Predictive probabilities of a SVGP with OVC to rollout conditional on these batches. Even in the non-Gaussian setting, OVC is able to adapt to new data without catastrophic forgetting. **Bottom row:** Variance of the latent function during the OVC rollout. The variances decay as we observe new data.

All variational GPs used GPyTorch’s whitened variational strategy. Unless otherwise specified, we normalized all inputs to $[0, 1]^d$ and standardized outputs to have zero mean and standard deviation one during the model fitting stage. We trained all models to convergence with an exponential moving average stopping rule using Adam with a learning rate of 0.1. We re-fit each model independently at each iteration. When plotting the median, we plot the 95% confidence interval around it following <https://www-users.york.ac.uk/~mb55/intro/cicent.htm>. Unless otherwise specified, all acquisitions were optimized with multi-start L-BFGS-B with 10 random restarts and 512 samples for initialization for up to 200 iterations with a batch limit of 5 following Balandat et al. [2].

Understanding Experiments

All understanding experiments, e.g. Figures 1, 6, 7, 8 were run on CPUs with Intel i5 processors. Computational costs were negligible to the cost of writing this paper.

Figure 1: We fit each non-Gaussian model using the ELBO. The Gaussian function is $f(x) = \sin(2|x| + x^2/2)$ with $n = 100$ and $n_{\text{test}} = 25$. For the GPCV model, we follow the model definition of Wilson and Ghahramani [82] and parameterize the scale of the Gaussian as a linear softplus transform, but we implemented a variational version, rather than the Laplace or MCMC implementations that are considered in the original paper. The data itself is a forward simulation of the well known SABR volatility model [30] with parameters $F_0 = 10$, $V_0 = 0.2$, $\mu = 0.2$, $\alpha = 1.5$, $\beta = 0.9$, $\rho = -0.2$. We model the scaled log returns and plot volatility rather than the latent function. We use $n = 250$ and $n_{\text{test}} = 150$, so that $T = 400$; we standardize the inputs. Here, to perform

Laplace approximations, we used PyTorch’s higher order AD software as deriving the gradients and Hessians would be tedious.

Knowledge Gradient on Branin: We used the Branin test function as implemented in BoTorch [2] with $n = 50$ and 25 inducing points, 8 fantasies per data point, 250 candidate points and a grid of size 15×15 . These were run on a single Nvidia Titan 24GB RTX. Computation took several minutes.

Incremental Learning on Protein: We followed the experimental protocol of Stanton et al. [70] but substituted in Matern-5/2 kernels with ARD instead of linear projections. The data comes from Dua and Graff [19]. The experiment is run over 10 random seeds and we show the mean and two standard deviations of the mean. Computation took several hours per trial.

Batch Knowledge Gradient Experiments

qEI and qNEI optimization used quasi Monte Carlo (QMC) integration with 256 random samples, while qKG optimization used QMC integration with 64 random samples (BoTorch defaults).

Hartmann6: Data comes from the Hartmann6 test function from https://github.com/pytorch/botorch/blob/master/botorch/test_functions/synthetic.py and the experiment is inspired by https://botorch.org/tutorials/closed_loop_botorch_only. These were run on CPUs on an internal cluster. Computation took several hours per trial. We used and 1000 randomly sampled candidate points to estimate the knowledge gradient.

Laser: Comparison scripts are from <https://github.com/ermongroup/bayes-opt/>. No license was provided. These were run on CPUs on an internal cluster. Computation took several hours per trial.

Preference Learning: Function is inspired by https://botorch.org/tutorials/preference_bo; we used noise of $\sigma = 0.1$ to make the function more difficult. The Laplace implementation comes from https://github.com/pytorch/botorch/blob/master/botorch/models/pairwise_gp.py. These were run on CPUs on an internal cluster. Computation took several hours per trial. qNEI optimization used QMC integration with 128 random samples, while qKG optimization used QMC integration with 64 random samples. Here, we used 3 random restarts and 128 raw samples for acquisition function optimization.

Active Learning Experiments

Malaria: Data is originally from Weiss et al. [81] under a creative commons 3 license, <https://malariaatlas.org/malaria-burden-data-download/#FAQ>. From the reference, the data is modelling predictions off of survey data and thus not human responses. For all models, we used Matern-1/2 kernels due to the lower smoothness and fixed noise models as variance is known. Comparison is to WISKI [70], with their code https://github.com/wjmaddox/online_gp which uses Apache License 2.0. These were run on a combination of Nvidia 32GB V100s and 48GB RTXes on an internal cluster. Here, we used 4 random restarts with 64 base samples to optimize the aquisition. Computation took several hours per trial.

Hotspot Modelling: Simulated data and comparison data is from https://github.com/disarm-platform/adaptive_sampling_simulation_r_functions. No license was provided for either. Our trials were run on AMD 32GB Mi50 GPUs on an internal cluster. Computation took close to eight hours per trial. We used tempering with $\beta = 0.1$ [38] and Matern-3/2 kernels for these models following the kriging setup in Andrade-Pacheco et al. [1]. Overall, we used 16 inner and outer samples for the entropy search objective, enumerating over all remaining test points to select a new point to query.

We note that the model fitting procedure of Andrade-Pacheco et al. [1] seems to possibly encourage test-set leakage as they seemingly use a random forest trained on all of the data, rather than on simply the first n observations. See the third from final paragraph in their description of spatial methods in that section. We do not follow this as we do not use any random forests.

TurBO Experiments

Rover: We use the opensource Turbo implementation from https://botorch.org/tutorials/turbo_1 and the rover function setup code from <https://github.com/zi-w/>

Ensemble-Bayesian-Optimization. Both are licensed under the MIT License. These were run on Nvidia 24GB RTXes on an eight GPU server. We repeated experiments 24 times. See the wall-clock time panels for estimates of computational budgets (about an hour). As not all trials reached exactly 40,000 iterations (due to cholesky decomposition errors, memory errors, and TurBO not restarting after 190 steps), we assume that the maximum achieved value was the best evaluation out to 200 steps to mimic the performance that one would see if using the method in practice. Early failures were only an issue for the exact GPs and then due to numerical instability, actually inspiring Figure 12a. As this truncation wreaked a bit of havoc with our timings, we only report the first 150 step timings in the main text (170 for Figure 13).

We used 500 data points and the same model classes for the conditioning experiment (Figure 12a). Error bars are two standard deviations of the mean over the 10 paths used.

For the global models experiment (Figure 12c), we used a combination strategy that first used half the batch with Thompson sampling (TS) to select the points and then used qGIBBON [54] to select the other half of the batch by setting the TS half of the batch as pending points. Performance using qGIBBON alone was about twice as slow and was slightly worse due to the lack of exploration that TS provides. This strategy also enforces that qGIBBON’s implementation actually uses fantasization and OVC, which would not natively have been the case without using the pending points. For the timings, we report the first 106 steps over 8 seeds.

MuJoCo: We use the codebase of Wang et al. [78] including their patched TurBO implementation with an optimization loop. This codebase is available from <https://github.com/facebookresearch/LaMCTS/tree/master/LA-MCTS> with a Creative Commons 4.0 License with the included, modified TurBO implementation following a non-commercial license. The MuJoCo experiments use mujoco-py (<https://github.com/openai/mujoco-py>, MIT License) and an institutional license key for MuJoCo itself [75]. These were run on a combination of Nvidia 32GB V100s and 48GB RTXes on an internal cluster. We repeated these experiments over 10 trials and computation took close to 14 hours for hopper (where one trial failed to reach 4000 samples for all methods but exact LTS), and several hours for swimmer.

On hopper, we struggled with wide variation in model fits, so we changed the regularization strategy on the base GP models to account for the high dimensional feature space. Inspired by Eriksson and Jankowiak [21], we continued using ARD Matern-5/2 kernels but placed HalfCauchy(τ) priors on the inverse lengthscales and then placed a HalfCauchy(1.0) prior on τ itself. Rather than using MCMC as Eriksson and Jankowiak [21] did, we used MAP to estimate both the lengthscales and τ .

D.3 Bayesian Optimization with the Knowledge Gradient

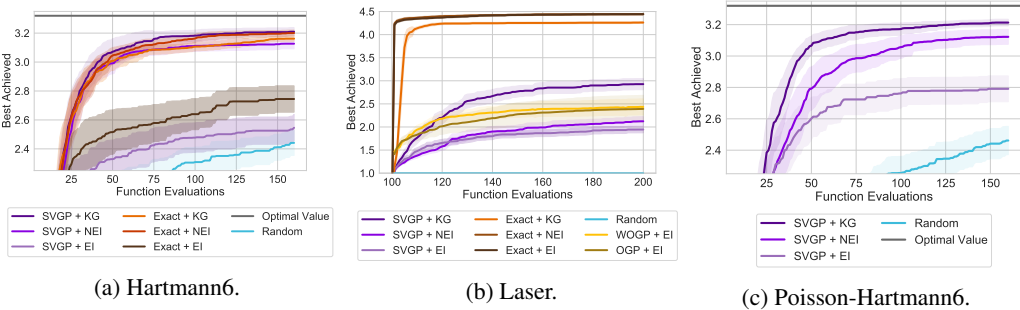


Figure 9: **(a)** Comparison to a broader suite of methods on Hartmann6, 1 constraint. **(b)** Comparison including BoTorch exact GPs and their acquisitions on the free electron laser problem. Comparing to the results in Figure 3 of McIntire et al. [51], these exact GPs vastly outperform their implementation, presumably due to advances in acquisition function optimization. **(c)** Hartmann6 test problem with count responses (Poisson likelihood). Only approximate inference can be used here, and qKG vastly outperforms qNEI.

In Figure 9, we present the results for a wider set of acquisition functions using the one-shot knowledge gradient on three test functions. These results complement Figure 3 and only include

these additional methods. Overall, qKG (with either an exact GP or a SVGP) generally performs best, followed by qNEI and then qEI.

In Figure 9a, we include results on the constrained Hartmann6 problem with random baselines as well as exact and SVGPs with expected improvement (EI). Exact and SVGPs with EI are significantly outperformed by the other, more advanced acquisitions, but do outperform a random baseline.

Figure 10: Best achieved values on Hartmann-6 for batch size, $q = 3$ for both NEI and KG for exact and SVGPs.

Noise Level	Acqf	Method	Best Value
0.1	NEI	Exact	3.19 (0.05)
0.1	NEI	SVGP	3.08 (0.06)
0.1	KG	Exact	3.17 (0.03)
0.1	KG	SVGP	3.13 (0.04)
0.5	NEI	Exact	3.20 (0.03)
0.5	NEI	SVGP	3.12 (0.06)
0.5	KG	Exact	3.15 (0.03)
0.5	KG	SVGP	3.21 (0.05)

In Figure 9b, we also show the results of exact GPs as well as an online GP [OGP, 16] with EI using the implementation of McIntire et al. [51]. Interestingly, all of the exact GPs significantly outperform their variational counterparts. This is quite surprising in some sense, as the true simulator is a weighted OGP with fixed hyper-parameters, and this method (WOGP + EI) performs much worse. Note that the random baseline makes no progress.

Finally, in Figure 9c, we display the results on constrained Hartmann-6 with Poisson observations, where each method outperforms random querying, but as expected SVGP + qEI, performs worse than qNEI and qKG.

Batch Size and Noise Level Ablation: In Tables 10 and 11, we display the final optimization results after 150 function evaluations on the Hartmann-6 test problem for varying levels of noise and for each acquisition. These results are over 20 trials and we display the mean maximum achieved value.

Overall, KG tends to outperform NEI at both low and noise levels, with both exact and SVGP models performing very similarly overall with the SVGPs getting a slight edge in the high noise setting. Furthermore, larger batch sizes tend to perform slightly better as the mean maximum achieved tends to have lower variation. Finally, higher noise levels tend to be somewhat harder to optimize as expected.

As we add more Gaussian noise into the function, we might a priori expect that qNEI should outperform qKG given the class of models. However, all things being held equal, a model that is more robust to the observed noise should tend to perform better, particularly if we are using more than just its mean and variance. Thus, SVGP models, by virtue of having more parameters to tune, tend to be more robust to the observed noise than the exact GPs.

D.4 Ablations on Rover

Figure 11: Best achieved values on Hartmann-6 for batch size, $q = 1$ for both NEI and KG for exact and SVGPs.

Noise Level	Acqf	Method	Best Value
0.1	NEI	Exact	3.14 (0.13)
0.1	NEI	SVGP	3.10 (0.10)
0.1	KG	Exact	3.20 (0.02)
0.1	KG	SVGP	3.18 (0.03)
0.5	NEI	Exact	3.10 (0.10)
0.5	NEI	SVGP	3.10 (0.14)
0.5	KG	Exact	3.12 (0.04)
0.5	KG	SVGP	3.16 (0.05)

Effects of LTS: To ablate the effects of rollouts and improved conditioning, we consider several step rollouts on the rover function as shown in Figure 12a. We find that performance is similar across depths. However, the conditioning of the resulting training data covariance is vastly improved when using OVC, as shown in Figure 12b. Taking these two results together, we see that in most cases, a tree depth of 4 should be enough to gain the improvements from rollouts without increasing the conditioning of the system too much.

Global models and SGPR: To further demonstrate time efficiency of using OVC in the context of even global models, we perform large batch BO with the recently introduced qGIB-

BON acquisition (a max value entropy search variant) but using half the batch with TS to enforce fantasization over the TS-acquired batch [54]. This strategy is significantly slower than TurBO;

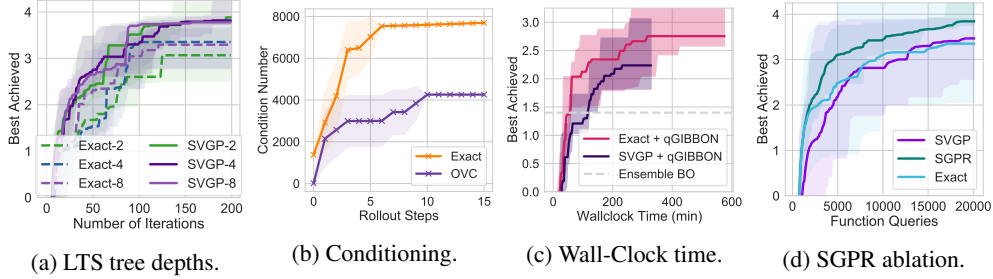


Figure 12: **(a)** Conditioning of exact and OVC conditioning across LTS tree depths on rover. **(b)** Performance of different rollout depths is similar, as the bigger gains are conditioning. **(c)** Time efficiency using global models. SVGPs are still a strong baseline. **(d)** Comparison with SGPR using pivoted cholesky initialization on rover. SGPR is competitive.

however, even in this setting using SVGPs is twice as fast, and achieves a similar result to the exact model, as shown in Figure 12c. Both are orders of magnitude faster than Ensemble BO, which uses batch max value entropy search and exact GPs with additive kernels [80, 79]. Ensemble BO takes at least several days of compute time [22]. Our result here compares very favorably to the (un-timed) results using SVGPs as well as exact GPs with ARD kernels that Wang et al. [79] also compared to, as neither of those methods reached reward values ≥ 1 on this problem, even after 35,000 steps.

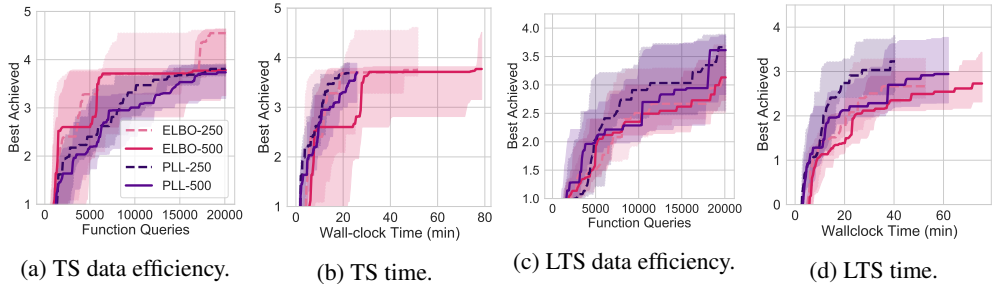


Figure 13: Inducing point ablation on rover **(a,b)** use Thompson sampling and **(c,d)** use rollouts.

Number of Inducing Points and Training Loss: Finally, in Figure 13 we ablate between training SVGPs with either 250 or 500 inducing points as well as the training loss, either the evidence lower bound (ELBO) or the predictive log likelihood (PLL), (see Appendix B.3 for further descriptions) on the $d = 60$ rover problem. We find that there is not a significant amount of difference between any of the four approaches whether using the ELBO or the PLL. In general, the PLL approaches are somewhat more quick to train (Figures 13b and 13b) in comparison to the ELBO models. They also tend to slightly outperform the ELBO-trained SVGPs when using LTS (Figure 13c) in terms of function efficiency, but perform similarly for standard Thompson sampling (Figure 13a). We leave a detailed benchmarking of these methods in the context of downstream tasks for future work.